https://doi.org/10.5194/egusphere-2026-1390
Preprint. Discussion started: 20 March 2026

A high-resolution perspective on climate drivers of lake stratification and phototrophic community dynamics in Late Glacial Central Europe

Petra Zahajská[1,2], María Luján García[3], Stella Birlo[3], Andrea Lami[4], Martina Stebich[5], Stan J. Schouten[1], Noé R.M.M. Schmidhauser[1], Bernd Zolitschka[3], Hendrik Vogel[6], and Martin Grosjean[1]

[1]Institute of Geography & Oeschger Centre for Climate Change Research, University of Bern, Bern, Switzerland
[2]Institute of Geology and Paleontology, Faculty of Science, Charles University, Albertov 6, Prague, 12843, Czechia
[3]Institute of Geography, University of Bremen, Bremen, Germany
[4]Water Research Institute, IRSA, CNR, Verbania, Italy
[5]Senckenberg - Leibniz Institution for Biodiversity and Earth System Research, Senckenberg Research Institute and Natural History Museum Frankfurt, Research Station of Quaternary Palaeontology, Am Jakobskirchhof 4, 99423 Weimar, Germany
[6]Institute of Geological Sciences & Oeschger Centre for Climate Change Research, University of Bern, Bern, Switzerland

Correspondence: Petra Zahajská (petra.zahajska@unibe.ch)

Abstract. Predicting the trajectory of aquatic deoxygenation under global warming requires a mechanistic understanding of lacustrine responses to rapid climate shifts. We investigated how climate-driven changes in catchment vegetation and local iron-rich lithology regulated lake stratification and ecosystem resilience in the maar lake Holzmaar (Central Europe). We focused on the Late Glacial, specifically on transitions during Dansgaard-Oeschger Event 1 (DOE-1; ca. 14,690–11,700 cal yr BP), a period of rapid natural warming and cooling that serves as an analogue for future high amplitude climate variation and for modern Arctic lakes undergoing rapid climate-driven transitions. Combining non-destructive hyperspectral imaging (HSI) of sedimentary pigments with high-resolution XRF geochemistry, we resolved parts of the ecosystem trajectory during DOE-1.

Ecological succession progress from a pioneer community of cyanobacteria to a stable anoxic late-successional community characterized by planktonic diatom *Stephanodiscus minutulus* and anoxygenic purple sulphur bacteria (PSB) in the photic zone. While regional warming (mean summer temperature increased ∼2.8°C) provided the physical potential for lake stratification, our data suggest that intense anoxia was primarily triggered by the expansion of *Betula* in the watershed. This afforestation stabilized the water column through wind shielding. The termination of the anoxic phase coincided with the onset of the Younger Dryas cooling and increased aridity, which effectively destabilized the existing stratification. While the shift from *Betula* to *Pinus* forest may have caused a change in the terrestrial-aquatic linkage, the primary driver of the transition was the physical forcing (lake mixing) of the climatic shift (cooling).

Geochemically, the lake exhibited remarkable resilience. Unlike carbonate-dominated systems prone to internal phosphorus loading, Holzmaar efficiently sequesters nutrients via a dual mechanism of reactive iron binding (authigenic vivianite) and stable mineral burial. The phosphorous trap prevents nutrient release by permanently sequestering P in the sediment, allowing rapid ecosystem recovery without delay once the specific climate and vegetation drivers shift. Our findings demonstrate that

https://doi.org/10.5194/egusphere-2026-1390
Preprint. Discussion started: 20 March 2026

in volcanic maar lakes, catchment vegetation characteristics and local lithology can modulate, and even override, the direct effects of climate warming on aquatic anoxia.

Keywords: varved lake sediment, hyperspectral imaging, sedimentary pigments, Holzmaar, XRF scanning

1 Introduction

Hypoxia and anoxia in freshwater ecosystems represent a critical global environmental challenge. The depletion of dissolved oxygen in bottom waters threatens aquatic biodiversity, alters nutrient cycling, and compromises water quality (Jenny et al., 2016; Woolway and Merchant, 2019). While often driven by anthropogenic nutrient loading in the Anthropocene, anoxia is also a natural feature of many deep lake systems, fundamentally linked to physical mixing regimes and climate forcing. However, predicting the trajectory of these systems under future warming remains difficult because separating the direct effects of temperature from the indirect effects of catchment change (land cover, nutrients) is challenging in modern, human-impacted landscapes.

The development of hypolimnetic anoxia typically follows a predictable cascade of physical and biogeochemical processes. Rising atmospheric temperatures increase the thermal stability of the water column, extending the duration of seasonal stratification and isolating deep waters from atmospheric oxygen exchange (Kienel et al., 2017). Simultaneously, warmer surface waters and enhanced nutrient fluxes stimulate primary production, increasing the export of organic matter (OM) to the hypolimnion. The microbial decomposition of this OM consumes the limited oxygen pool, eventually driving the system toward anoxia once physical re-aeration is inhibited. This coupling has been well-documented in high-resolution studies of varved sediments across Central Europe. For instance, in Lake Żabińskie and Lake Jaczno (NE Poland), seasonal anoxia is tightly coupled to productivity cycles and physical mixing thresholds (Zander et al., 2021a; Żarczyński et al., 2019; Butz et al., 2017). Similarly, studies from Swiss lakes have demonstrated how changes in mixing regimes directly influence sediment phosphorus retention (Tu et al., 2020). In many modern temperate lakes, this cycle is seasonal: anoxia builds up during the stratified summer and autumn and is broken only when surface cooling and wind stress induce deep convective mixing in winter or spring (Schwefel et al., 2016).

The Late Glacial period (Dansgaard-Oeschger event 1: Greenland Interstadial 1, GI-1, ca. 14,690–12,900 cal yr BP, Greenland Stadial 1, GS-1, 12,900-11,700 cal yr BP) offers a unique natural laboratory to test these mechanisms over centennial timescales. We hypothesize that Late Glacial lakes in Central Europe serve as valuable analogues for modern Arctic lakes, where rapid warming and catchment stabilization fundamentally alter aquatic states. In this framework, the rapid Bølling warming triggered a long-term phase of stratification and anoxia, driven not just by temperature, but also by the associated expansion of catchment vegetation, which shielded the lake from wind mixing (Makri et al., 2020; Tu et al., 2021). Further, the cooling of the Younger Dryas mimics the transition back to a high-latitude or polar mixing regime, theoretically breaking stratification and re-oxygenating the hypolimnion. However, the resilience of lake ecosystems to these shifts, specifically whether they recover immediately or experience a delayed recovery, depends on internal biogeochemical feedbacks.

https://doi.org/10.5194/egusphere-2026-1390
Preprint. Discussion started: 20 March 2026

Moreover, we hypothesize that these Late Glacial climate oscillations represent shifts between distinct thermal states, analogous to the gradient between modern temperate-stratified and high-latitude lakes. The Bølling-Allerød warming initiated a phase of stable, prolonged stratification and anoxia, supported by the forest expansion documented in temperate systems (Makri et al., 2020; Tu et al., 2021). The Younger Dryas cooling represents a shift toward an Arctic-type thermal regime. Despite the transition from *Betula* to *Pinus* in the catchment, the decrease in mean annual temperatures and humidity, combined with shortened growing season, likely promoted more frequent lake mixing. This shift mimics the seasonal behaviour of modern high-latitude lakes where reduced thermal gradients facilitate hypolimnion re-oxygenation. However, the resilience of lake ecosystems to these shifts, specifically, whether they recover immediately or exhibit delayed recovery, depends on internal biogeochemical feedbacks (Schmidt et al., 2002; Lone and Balakrishna, 2023; Schouten et al., 2026).

A key uncertainty lies in how catchment characteristics (lithology, topography, land cover and soils) modulates this response. While physical thresholds for anoxia have been established, such as the ca 80% arboreal pollen threshold for wind shielding at Soppensee, Moossee and Żabińskie (Makri et al., 2020; Zander et al., 2021b; Schouten et al., 2026), a critical gap remains regarding the biological and geochemical response. Previous studies at Holzmaar have successfully reconstructed sediment yields (Zolitschka, 1998) and broad diatom community shifts (García et al., 2022), yet the specific aquatic primary production, algal community shifts and elemental (nutrient) cycling remain unresolved.

Here, we investigate Holzmaar (Westeifel Volcanic Field, Germany) to resolve the coupling between climate forging, catchment vegetation, and the internal drivers of eutrophication, stratification and aquatic anoxia. The Eifel region is uniquely suited for this, as recent quantitative temperature reconstructions using branched GDGTs provide a specific local thermal history (Zander et al., 2024), allowing us to discriminate local climate forcing from hemispheric trends (NGRIP). We address the following research questions by combining high-resolution hyperspectral imaging (HSI) and HPLC-derived pigment concentrations with XRF geochemistry and sequential extractions of P, Mn, and Fe. These biogeochemical data are further supported by pollen, diatom, and temperature records to address three key questions:

1. How do phototrophic communities succeed one another during the onset of rapid warming followed by stratification?
2. Does the iron-rich catchment provide a distinct geochemical buffer (e.g., efficient P-retention) that distinguishes volcanic lakes from carbonatious systems?
3. Is the ecosystem state reversible? Specifically, does the lake exhibit hysteresis (delayed recovery) after the climatic driver is removed?

By comparing the trajectory of Holzmaar to regional records (Tu et al., 2021; Makri et al., 2020), we identify the specific roles of catchment vegetation and iron availability in regulating lake resilience.

https://doi.org/10.5194/egusphere-2026-1390
Preprint. Discussion started: 20 March 2026

2 Material and methods

2.1 Study site

Holzmaar (50°7'N, 6°53'E; 425 m a.s.l.) is a maar lake located in the Westeifel Volcanic Field, Germany (Zolitschka et al., 2000). The catchment of Holzmaar is a region characterized by the iron-rich Devonian bedrock and also known for its iron deposits associated to volcanism (Schmincke, 2007; Lottermoser et al., 1997; Schmitt et al., 2023). The lake basin exhibits a circular morphology with a small surface area (58,000 m^2) relative to its maximum depth of 20 m (Negendank and Zolitschka, 1993). This specific crater morphometry naturally predisposes the lake to meromixis and high sensitivity to climatic forcing (Lami et al., 1994). Due to its great depth and steep basin slopes, stable thermal stratification can develop and inhibit deep-water mixing (Brauer et al., 2001) below 10-15 m. Under modern conditions, the lake stratifies from May to December with a thermocline/chemocline typically situated at 6–8 m depth, resulting in seasonal hypolimnetic anoxia that favours the preservation of annually laminated (varved) sediments (Zolitschka, 1998; García et al., 2022).

This study focuses on the Dansgaard-Oeschger Event 1 (ca 14,690–11,700 cal yr BP). This interval is characterized by the rapid Bølling warming, which drove a vegetation succession from steppe tundra to shrub tundra, and finally to *Betula* and *Pinus* forests during the Allerød (Litt and Stebich, 1999). Coincident with this catchment stabilization, the lake underwent a transition from ultra-oligotrophic to mesotrophic conditions. This shift is marked by the replacement of benthic *Staurosira construens* with planktonic *Stephanodiscus minutulus* and increased accumulation of organic carbon, primary production (based on $\delta^{13}C$ and biogenic silica (Zolitschka et al., 2000; García et al., 2022; Lücke et al., 2003). The subsequent Younger Dryas cooling (ca. 12,750–11,500 cal yr BP) interrupted this trajectory, leading to forest opening and a temporary reduction in aquatic primary production (Brauer et al., 2001).

2.2 Coring, physical and chemical properties

Four parallel sediment cores (HZM19-07, HZM19-08, HZM19-10, HZM19-11) were recovered in August 2019 from the centre of Holzmaar at 18–19 m water depth using a UWITEC piston corer (García et al., 2022) and compiled to a composite sediment record (Birlo et al., 2023). The X-ray fluorescence (XRF) core scanning for elemental composition with a Cr X-ray tube, high-resolution logging of magnetic susceptibility, and determination of total organic carbon (TOC), total nitrogen (TN), and biogenic silica (BSi) data at a relatively low resolution of 16 cm (García et al., 2022) were complemented by hyperspectral scanning data acquired at the University of Bern and higher resolution diatom stratigraphy (every 4 cm) established at the University of Bremen.

Sedimentary pigments were quantified non-destructively using hyperspectral imaging with a Specim PFD-CL-65-V10E line scan camera operating in the visible and near-infrared range (VNIR, 400–1000 nm). The camera set-up (frame rate: 8 Hz, exposure: 120 ms) delivered data with a spectral resolution of 1.56 nm and a spatial resolution of 80 μm (pixel size). The hyperspectral data were normalized using a white reference ($BaSO_4$) and dark reference (closed camera aperture).

Hyperspectral data post processing was performed using napari-sediment (Witz and michaelh00, 2025), an open-source Python plugin for the napari image viewer, specifically designed for interactive analysis of hyperspectral sediment core imagery.

https://doi.org/10.5194/egusphere-2026-1390
Preprint. Discussion started: 20 March 2026

napari-sediment provides an integrated workflow that combines visualization, preprocessing, dimensionality reduction, and spectral analysis in a single graphical user interface following the data processing proposed in Butz et al. (2015) and further described in the Appendix A. Relative Absorption Band Depth (RABD) indices were calculated to quantify absorption troughs associated with specific photopigments. Following established protocols by Butz et al. (2015), Schneider et al. (2018) and Zander et al. (2022), absorption trough minima were identified at the following wavelengths:

- 619 nm – Phycocyanin from cyanobacteria (Wienhues et al., 2025)
- 670 nm – Total chlorophyll *a* (Tchl) from oxygenic phototrophs (Rein and Sirocko, 2002)
- 715 nm – bacteriopheophytin *e* (bphe *e*) from green sulphur bacteria (GSB) (Zander et al., 2023)
- 845 nm – bacteriopheophytin *a* (bphe *a*) from purple sulphur bacteria (PSB) (Butz et al., 2015)

RABD index values were calculated using the formula of Butz et al. (2015):

$$\mathrm{RABD}_\lambda = \frac{\frac{\mathrm{X_{right}} \cdot \mathrm{R_{left}} + \mathrm{X_{left}} \cdot \mathrm{R_{right}}}{\mathrm{X_{right}} + \mathrm{X_{left}}}}{\mathrm{R}_\lambda} \tag{1}$$

where R_λ is the reflectance at the absorption minimum (λ), X stands for the number of bands from the left side of the trough to λ ($\mathrm{X_{left}}$), or from the right side to the λ ($\mathrm{X_{right}}$), and $\mathrm{R_{left}}$ and $\mathrm{R_{right}}$ are the reflectance values at start and end of the reflectance trough.

RABD index values from hyperspectral imaging were calibrated to absolute pigment concentrations measured by spectrophotometry using linear regression models. Calibration samples were selected to represent the full range of pigment concentrations present in the core following a normal distribution.

2.3 Chronology

The chronology for the Holzmaar composite profile is based on the Bayesian age-depth model established by Birlo et al. (2023). This model integrates the original high-resolution varve chronology of Zolitschka et al. (2000) with radiometric dating to optimize the age transfer to the new HZM19 sediment cores. The age model is stratigraphically anchored by the Laacher See Tephra (LST) (Reinig et al., 2021), a distinct isochron visible in the lithology (Cluster IV, HClust, dark red in Fig. 1), which serves as a critical time marker for the Allerød. This varve-based framework provides annual to sub-decadal temporal resolution, allowing for precise correlation of biogeochemical changes during the Late Glacial period (ca. 14,690–11,700 cal yr BP).

The biostratigraphy for the Holzmaar record follows the regional pollen stratigraphy (Lang et al., 2023; Litt and Stebich, 1999). In this study, we adopt the term Pleniglacial (Birlo et al., 2023; García et al., 2022) to describe the period corresponding to the Oldest Dryas in Swiss and South German biostratigraphies, e.g., Lotter and Kienast (1992). Similarly, the period referred elsewhere as the Meiendorf is here termed the Bølling. The subsequent sequence follows the regional standard: the Older Dryas

https://doi.org/10.5194/egusphere-2026-1390
Preprint. Discussion started: 20 March 2026

stadial, the Allerød interstadial with the Laacher See Tephra, the Younger Dryas stadial. The exact dates of their stratigraphic boundaries are from Birlo et al. (2023).

2.4 Sedimentary pigment quantification

Further, we calibrated hyperspectral indices to absolute pigment concentrations measured by spectrophotometer. These independent pigment measurements were performed using UV-visible absorption spectrophotometry (Shimadzu UV-1800) and high-performance liquid chromatography (HPLC). Pigment extractions were performed on 1.5 to 0.5 g wet and homogenized sediment subsamples using 100% HPLC-grade acetone following the protocol of Lami et al. (1994); Pniewski (2020); Strickland and Parsons (1972). In short, we extracted pigments by adding 5 to 13 ml acetone in several steps (2-3 ml per step), keeping the samples in dark and at 4°C conditions over night, or 30 minutes in -4°C between the extraction steps, until the supernatant was visually colourless. The samples were always centrifuged (3500 rpm, 10 min), the supernatant was decanted and filtered through hydrophobic PTFE 0.22 μm filters (13 mm syringe filters) and stored at -20°C in darkness until analysis.

For spectrophotometric analysis, pigment extracts were measured using a UV-visible spectrophotometer (wavelength range 350–900 nm, spectral resolution 0.1 nm) with 1 cm path length PP cuvettes. Total chlorophyll *a* and derivatives (pheophytins, pheophorbides) were quantified spectrophotometrically using absorption at 663 nm and 665 nm and translated to concentration using the Lambert-Beer law and the extinction coefficient for bulk green pigments (chlorophylls, pheophytins and pheophorbides) in 90:10 Acetone:Water solution ($\epsilon = 80.8 \cdot 10^{-3}\,\mathrm{l \cdot mg^{-1} \cdot cm^{-1}}$, adjusted after Jeffrey and Humphrey, 1975). Total bacteriopheophytin *a* concentration was quantified using the absorption peak at 745 nm in 90% acetone ($\pm$10% of water originating from the wet sediment), and applying the specific absorption coefficient ($\epsilon = 52.9 \cdot 10^{-3}\,\mathrm{l \cdot mg^{-1} \cdot cm^{-1}}$, Fiedor et al., 2002).

Pigment extracts (100 μL aliquots) were analysed using a Dionex Ultimate 3000 series reverse-phase HPLC system equipped with a C18-ODS column (Agilent Omnisphere-5) and a Diode Array Detector (DAD-3000RS), following the method of Lami et al. (1994) described in detail in Schouten et al. (2025). Chromatogram peaks were integrated using Chromeleon 7.2 (ThermoFischer Scientific®) with a Gaussian fit approach. Individual pigments were identified based on retention times and absorption spectra, and quantified using pre-determined linear regression coefficients for authentic standards (Schouten et al., 2025).

To calibrate hyperspectral imaging (HSI) data with pigment concentrations measured by spectrophotometry, we employed a proxy-proxy linear regression model. After testing for normality using Shapiro-Wilk tests and screening for outliers using Rosner's test, we established linear relationships between RABD indices and pigment concentrations. For total chlorophyll (TChl), we fitted the model:

$$\mathrm{TChl}(\mu\mathrm{g \cdot g^{-1}}) = 467.6 \times \mathrm{RABD}_{670} - 467.1 \tag{2}$$

with R^2 = 0.92, p = $4.6 \cdot 10^{-19}$, RMSEP = $3.25 \mu g \cdot g^{-1}$, (Fig. A1).

For bacteriopheophytin *a* (Bphe *a*), we fitted:

$$\mathrm{Bphe\ } a(\mu\mathrm{g \cdot g^{-1}}) = 131.3 \times \mathrm{RABD}_{845} - 129.2 \tag{3}$$

https://doi.org/10.5194/egusphere-2026-1390
Preprint. Discussion started: 20 March 2026

with R^2 = 0.82 p = $4.6 \cdot 10^{-13}$, RMSEP = $0.97 \mu g \cdot g^{-1}$ (Fig. A2). These calibration equations were then applied to the entire HSI dataset to generate spatially-resolved pigment concentration maps.

2.5 Diatoms

Diatom samples were prepared from 50 freeze-dried subsamples collected at discrete 4 cm intervals along the composite sediment profile. An aliquot of each sample was oxidized with 30% H_2O_2 and heated in a water bath at approximately 80°C for 2-5 minutes to eliminate organic matter, following standard methods. Samples were then rinsed repeatedly with distilled water until reaching neutral pH, and permanent slides were mounted using Naphrax mounting medium. A minimum of 400 diatom valves per slide were counted using light microscopy (Olympus CX40 with Plan Ach 100X/1.25 immersion objective and Zeiss Axioplan with Plan Neofluar 100X/1.30 immersion objective equipped with differential interference contrast) to calculate relative abundances and absolute concentrations (valves per gram dry sediment) using a modified evaporation tray method. Diatom identification followed standard European floras, and diatom accumulation rates were calculated by multiplying total diatom abundance by sediment accumulation rates derived from the varve chronology.

2.6 Sequential extraction of P, Mn, and Fe

Sequential extraction was performed using a modified protocol from Lukkari et al. (2007) and Scholtysik et al. (2022) to differentiate sedimentary P, Fe, and Mn into chemically distinct pools. The extraction scheme defined four operational fractions: (1) **F1** (labile/porewater), extracted with 0.46 M NH_4Cl; (2) **F2** (redox-sensitive), extracted with 0.11 M Bicarbonate-Dithionite (BD); (3) **F3** (Al-bound/organic/hydroxides), extracted with 1 M NaOH; and (4) **F4** (calcium-bound/residual), extracted with 0.5 M HCl. The extracts were analysed using ICP-MS (Agilent Series 7600) in a 1% HNO3 matrix-matched solution at the University of Bern. The concentrations of Fe, Mn and P were calculated based on external calibration curves from IPC-MS multi-element standard.

We acknowledge that strict anaerobic integrity could not be maintained during core transport and subsampling. Consequently, labile reduced species (e.g., porewater Fe^{2+}, authigenic vivianite) susceptible to rapid oxidation may have shifted from their target fractions (F1 or F3) into the reducible fraction (F2). Therefore, we adopt a conservative operational definition, where we interpret Fraction 2 not as specific oxides, but as the total reactive pool, encompassing both original oxides and secondary oxidation products of authigenic minerals. To infer the original mineralogical hosts of phosphorus, we evaluate the molar Fe:P stoichiometry of this reactive pool, rather than relying on the operational separation of F1 and F2 alone.

2.7 Pollen and external data

To find the link of our in-lake biogeochemical data with the external drivers, we compiled existing pollen data of Holzmaar from the literature and databases (Litt and Stebich, 1999; Litt, 2001; Litt et al., 2009; Litt, 2010, 2025). To synchronize these records with our 2019 chronology, individual core sections from the 1992 campaign (HZM92 1a–6u, 2b–5o, 2b–5u) were correlated to the 2019 composite depth using visual lithostratigraphic tie-points and then stacked with the 1996 composite

https://doi.org/10.5194/egusphere-2026-1390
Preprint. Discussion started: 20 March 2026

record (see Appendix B for full methodological details). The Holzmaar high-resolution pollen record covers only the period from 15,000 to 13,250 cal yr BP, and thus the trends for *Betula*, *Pinus*, and non-arboreal pollen (NAP) from 13.250 to 11,750 cal yr BP were modelled using the high-resolution record from the nearby Meerfelder Maar (Litt and Stebich, 1999, 2001). Missing values were reconstructed by applying scaling factors derived from the linear relationship between the two lakes during their overlapping stratigraphy (code is available as a part of the workflow at GitHub/Renku (Zahajská, 2026).

Moreover, we generated the annual, July and January insolation curve for the location of Holzmaar, with the resolution of 50 years from -50 to 15,950 cal. yr BP using the model of Laskar et al. (2004). To further constrain the temperature proxy, we used the chironomid-based July temperature reconstruction for Gerzensee (Lotter et al., 2012) as well as for Egelsee (Larocque-Tobler et al., 2009; Kaufman et al., 2020). We also utilized the regional GDGT-based temperature reconstruction from the Eifel, including Holzmaar (Zander et al., 2024). Lastly, we included the North GRIP δ^{18}O (NGRIP Members, 2004) and ice-core dust records (Ruth et al., 2003; Gkinis et al., 2014) into our set of external variables. These datasets demonstrate a clear seasonal pattern in dust concentrations that correlate with climatic variations.

The very first step was to test the relationship of the external variables and reduce the dimensionality. We conducted PCA on z-scored data and established a correlation matrix (Fig. A3). Only a selection of variables (winter insolation, $\delta^{18}O_{NGRIP}$ and dust data, GDGT-derived temperature, chironomid-inferred July temperature from Gerzensee, Holzmaar *Betula*, *Pinus* and non-arboreal pollen and XRF Ca and Ti) was used for further RDA analysis with our pigment data. The full workflow is available on Renku/GitHub (Zahajská, 2026) and fully linked to the dataset at Zenodo.

2.8 Data analysis

High-resolution XRF core scanning data were normalized using centred log-ratio (CLR) transformation to address the closed-sum constraint inherent to compositional data and minimize matrix effects (Weltje and Tjallingii, 2008; Bertrand et al., 2024; Aitchison, 1982). Hyperspectral imaging indices were calibrated against discrete spectrophotometer bulk pigment measurements using linear regression, as described above, enabling the quantification of sedimentary pigment concentrations at high temporal resolution throughout the core. To facilitate multi-proxy comparison, all datasets were interpolated to a common temporal resolution using Gaussian kernel smoothing.

Hierarchical cluster analysis (Ward's D2 method with Euclidean distance) and principal component analysis (PCA) were applied to the CLR-transformed XRF data to identify geochemical facies, with optimal cluster numbers determined through silhouette analysis. HPLC-derived pigments were grouped based on Pearson correlation coefficients of their downcore concentration profiles, and taxonomic assignments to algal and bacterial producer groups (e.g., cyanobacteria, green algae, diatoms, cryptophytes, purple sulphur bacteria) were made following established pigment biomarker literature (see Table A1).

Prior to redundancy analysis (RDA), predictor variables were pre-selected based on Pearson correlation matrices and PCA of external environmental variables to reduce collinearity and identify the most informative drivers. Final variable selection was performed using forward selection (ordistep function in the R package vegan) with permutation-based significance testing. The full workflow is available on Renku/GitHub (Zahajská, 2026) and fully linked to the dataset at Zenodo.

https://doi.org/10.5194/egusphere-2026-1390
Preprint. Discussion started: 20 March 2026

3 Results

3.1 Lithology

The unconstrained hierarchical clustering of XRF data resulted in five distinctive clusters (Fig. 1 and A4) separating more allochthonous sediment (Ti, K, Zr, Al) from autochthonous sediment (Ca, S, inc/coh). In combination with the hyperspectral data, we interpret the clusters as follows (Fig. 1): Cluster I (lime-green) corresponds to clayey silts with low pigment abundance at the bottom of the core, followed by cluster II inter-layered with cluster three (orange, dark blue) representing the varved section of diatoms (Si/Ti) and organic matter (inc/coh, RABD620, the total chlorophylls, bacteriopheophytin *a*). Cluster IV (dark red) is specific for the LST followed by organic rich section of cluster III (dark blue). The core top is classified as cluster V (light blue), which carries similarities with cluster I and is mainly minerogenic.

Similar separation is observed in the PCA (Fig. A4), where PC1 (45.3%, Fig. 1 and A4) separates the XRF data between allochthonous (positive) and autochthonous (negative) sediment sources. PC2 (11.5%) represents the division between minerogenic (negative) vs organic matter and redox sensitive (positive) elements in the sediment record.

Lastly, CONISS clustering was used to explore the clusters constrained with depth. Similarly to the unconstrained hierarchical clustering, five clusters were defined, which coincide well with the previously published lithology (Zolitschka, 1998).

3.2 Primary producer communities

The data of sedimentary pigments were examined using a heatmap, where individual pigments, representing a group of primary producers, were clustered based on their time-series similarities using correlation (Fig. 2). This clustering resulted in three different primary producer communities (pigment groups): (1) Pioneers, (2) Secondary colonisers and (3) Diatoms + purple sulphur bacteria (Fig. 3). The statistical separation of these communities and their distinct stratigraphic evolution is further visualized in the PCA trajectory (Fig. A5).

The first pigment group, pioneers, is composed mainly of cyanobacteria (Fig. 3), but also green algae, cryptophytes, silicifiers, red blooming algae, purple non-sulphur bacteria and green sulphur bacteria are present in the lake (Fig. 2). The presence of benthic species of diatoms, such as *Staurosira construens*, supports the low lake-level conditions (Negendank and Zolitschka, 1993). Further, the presence of the planktonic or periphytic *Pantocsekiella ocellata*, which thrives in oligotrophic waters with low phosphorous concentrations and a stratified water column (Vossel et al., 2015), aligns with the presence of anoxygenic phototrophic green sulphur bacteria in the photic zone (isorenoratene and chloraxanthin, Fig. 2). Further, we do not observe any formation of the redox sensitive element fraction of Mn (Fig. 3), P, or Fe (Fig. A6). This very diverse aquatic primary producer community occupied the lake during the relatively colder Pleniglacial period and was gradually replaced in the early Bølling by the community of secondary colonizers.

The pigment group of secondary colonizers developed in the lake at the onset of the Bølling warming (14,443 cal yr BP, Birlo et al. (2023)) as indicated by the peak in green algae (total chlorophylls and pigment group 2, Fig. 3), cyanobacteria as well as purple non-sulphur bacteria (OH-spheroidine, Fig. 2) and green sulphur bacteria (bacteriochlorophyll *a*). At the same time, the

https://doi.org/10.5194/egusphere-2026-1390
Preprint. Discussion started: 20 March 2026

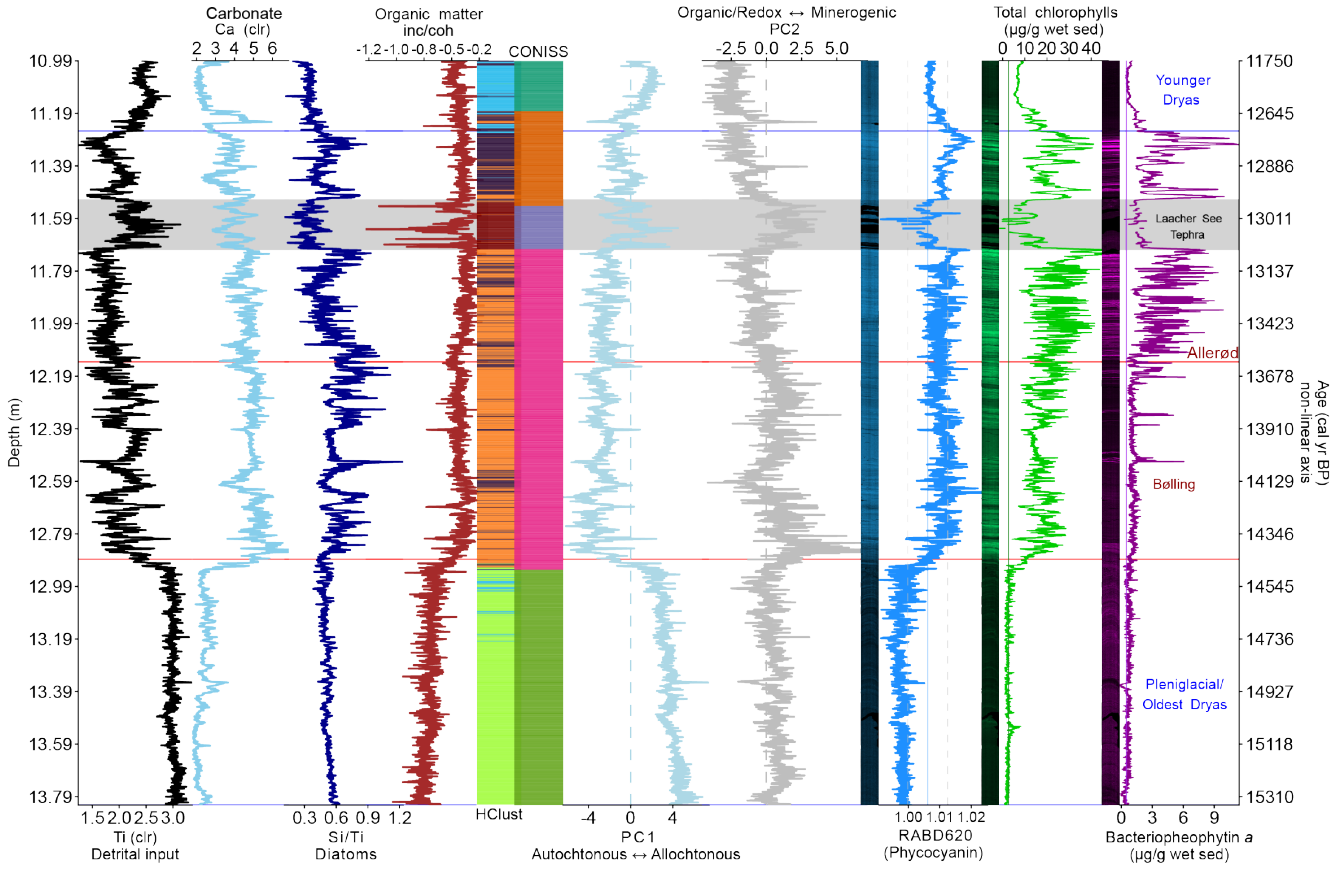

Figure 1. Selection of data from non-destructive high-resolution methods presenting the Holzmaar paleoenvironmental record plotted against depth (left axis) and time (non-linear right axis). The panels display geochemical proxies for detrital input (Ti clr) and carbonate (Ca clr), relative diatom abundance (Si/Ti), and organic matter (inc/coh). Statistical analyses include hierarchical clustering (HClust and CONISS) defining stratigraphic zones, and Principal Component Analysis. PC1 (45.3%) indicating autochthonous vs. allochthonous input; PC2 (11.5%) is reflecting organic (redox) conditions vs. minerogenic input. An intensity colour map of hyperspectral indices is shown alongside pigment proxies for cyanobacteria (RABD620), total chlorophylls, and purple sulphur bacteria (bacteriopheophytin *a*). Vertical lines are representing the limit of quantification. Major biozones following Birlo et al. (2023): Pleniglacial, Bølling, Allerød, and Younger Dryas are indicated on the right and marked by red and blue horizontal lines. The gray horizontal band highlights the position of the Laacher See Tephra (LST).

planktonic diatom *Stephanodiscus minutulus* appears in high abundances, supporting the water column deepening (Negendank and Zolitschka, 1993). Benthic diatoms, such as *Amphora indistincta Pseudostaurosira brevistriatta*, *Pseudostaurosira robusta* and *Staurosiella lapponica*, occupy the benthic and periphytic niche which is abandoned by the Pleniglacial species (Fig. A7). The composition of this community suggests that the lake was partly nutrient limited, likely in nitrogen. The gradually increasing reactive manganese pool (F2+F3) suggests, at least seasonally, oxygenated lake bottom waters (Fig. A6).

https://doi.org/10.5194/egusphere-2026-1390
Preprint. Discussion started: 20 March 2026

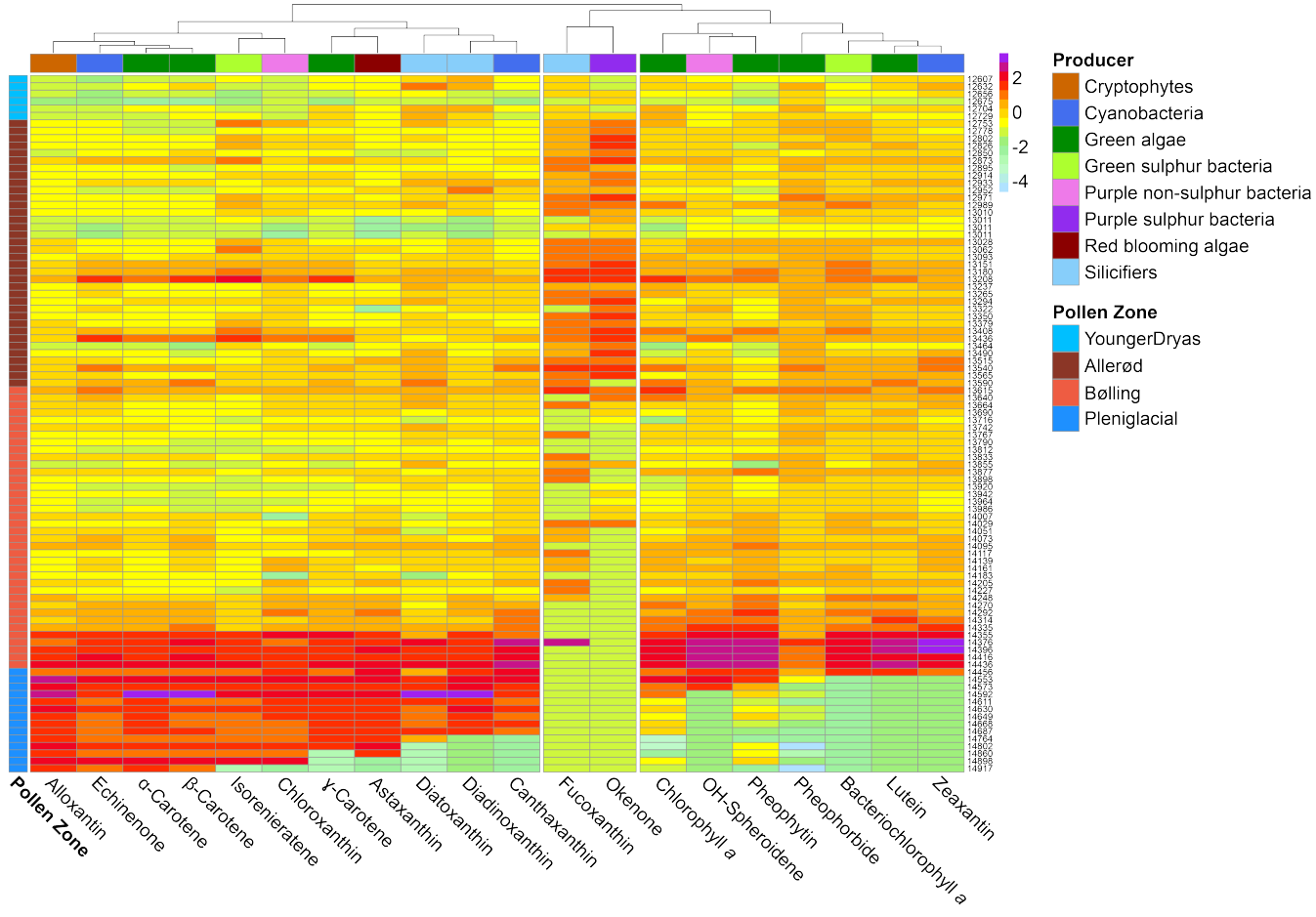

Figure 2. Stratigraphic heatmap and hierarchical clustering of sedimentary pigment assemblages. The heatmap displays the relative abundance (z-score normalized) of identified pigments across the sediment profile. Rows represent individual sediment samples (with ages in cal yr BP on the right), colour-coded by stratigraphic zone (left bar). Columns represent individual pigments, categorized based on their producer in the colour-coded top bar. The correlation-based clustering (top dendrogram) reveals three distinct ecological clusters. The left cluster contains pigments associated with the pioneer community (e.g., echinenone, canthaxanthin, alloxanthin and isorenieratene), which show high relative abundances in the Pleniglacial (bottom rows). The middle cluster contains pigments defining the late-successional community (okenone and fucoxanthin), which exhibit peak abundances during the Allerød (middle-upper rows). The right cluster represents secondary colonisers including green algae, cyanobacteria and green sulphur and purple non-sulphur bacteria, peaking in the early Bølling.

https://doi.org/10.5194/egusphere-2026-1390
Preprint. Discussion started: 20 March 2026

Finally, the pigment group of the late-successional community established during the Allerød and is dominated by the planktonic diatom *Stephanodiscus minutulus* and purple sulphur bacteria (okenone, bacteriopheophytin *a*). The high concentrations of okenone are particularly significant, as they indicate the development of stable, long-term euxinic conditions (anoxic and sulphidic) extending into the photic zone. This community structure remained remarkably stable throughout the Allerød, showing no substantial shifts in composition even following the deposition of the LST. Although the LST event introduced a significant amount of iron and silica, as well as changes in the light penetration, the established dominance of the okenone-producing *Chromatiaceae* suggests that the presence of persistent anoxia in the lake was sufficient to buffer the ecosystem against this disturbance, maintaining the strong seasonal stratification required for these sulphur bacteria to thrive.

3.3 Redox sensitive fractions of Mn, P and Fe

The sequential extraction data differentiates the available/reactive pools of Mn, P and Fe under changing redox conditions and anoxia. All extracted fractions are shown in the supplementary data (Fig. A6). Based on these profiles, we focus on Fraction 2 (F2) to represent the total reactive pool of Mn, Fe and P available for remobilization from the sediment during lake stratification.

Overall, the most abundant fraction for all three elements was the residual/carbonate-bound fraction (F4), which is dissolved only at low pH. The second most abundant fraction was the reactive F2, which represents phases readily dissolvable under reducing conditions.

Total manganese concentrations were highest in the Pleniglacial sediments. With the onset of the Bølling and the increasing concentrations of okenone during the Allerød, the reactive fraction of Mn (F2) shows a decreasing trend (Fig. 3), consistent with release from the sediment to the anoxic water column (reductive dissolution). Only after the LST (LST) we observe a distinct increase in the Mn reactive pool sequestered in sediments (Fig. A6).

Reactive iron (F2) and phosphorus (F2) display strong stratigraphic covariance throughout the record. Fe is closely coupled with P within this reactive fraction, with the molar Fe:P ratio of F2 stabilizing at $\sim$1.5 throughout the Bølling and Allerød (Fig. A6). This value corresponds to the 3:2 stoichiometry of authigenic vivianite ($Fe_3(PO_4)_2$, Nriagu (1972)), providing strong evidence that the reactive phosphorus pool is sequestered as vivianite rather than merely adsorbed onto iron oxides (which typically yields ratios $>$2, Slomp et al. (1996); Jensen et al. (1992)). While vivianite is frequently below bulk XRD detection limits, this consistent stoichiometric coupling in the reactive pool is a widely accepted diagnostic tool for identifying its presence and role in phosphorus sequestration in lacustrine settings (O'Connell et al., 2015; Rothe et al., 2016).

Following the LST, the lake was geochemically enriched by the influx of volcanic material. Fe and Mn concentrations in the reactive fraction (F2) increase significantly while P remains stable, resulting in fluctuating Fe:P ratios and an excess of reactive iron relative to phosphorus. This mineral influx effectively transformed the lake into an even more efficient phosphorus trap. By locking phosphate into stable mineral phases such as vivianite, the sediment acts as an efficient trap that prevents nutrient release back into the water column. This mechanism eliminates the internal loading effect common in carbonate-dominated lakes, allowing the ecosystem to recover quickly rather than being held in a prolonged anoxic state by legacy phosphorus.

https://doi.org/10.5194/egusphere-2026-1390
Preprint. Discussion started: 20 March 2026

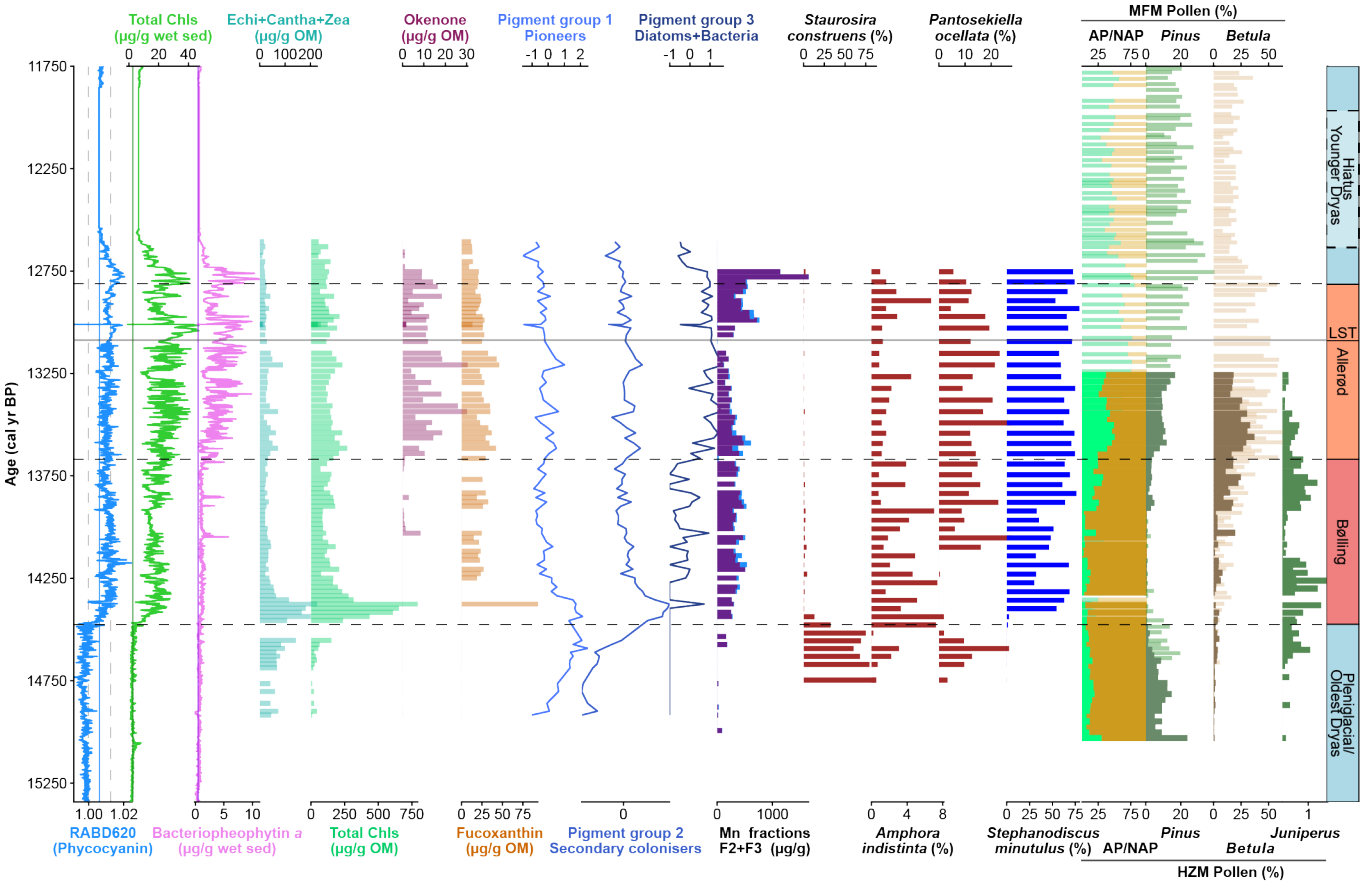

Figure 3. Stratigraphic variation of hyperspectral imaging data, selected sedimentary pigments, pigment communities derived from correlation (see Fig. 2), selected redox fractions (Mn), selected diatom species and pollen in Holzmaar (and Meerfelder Maar) (Litt and Stebich, 1999; Litt et al., 2009; Litt and Stebich, 2001; Litt, 2025, 2010). Downcore profiles of relative abundance of phycocyanin as RABD620, with solid line representing the mean value and dashed lines $\pm 1\sigma$, calibrated hyperspectral imaging bulk pigments data (expressed as [μg^{-1} g wet sediment]) with the limit of quantification as a solid vertical line, and HPLC-analysed pigment concentrations (expressed as [μg^{-1} OM]) are plotted against age (cal yr BP). The pigment communities are plotted as z-scores. Benthic diatoms are plotted in dark red and planktonic diatoms are displayed in blue. Arboreal pollen is show in light green and non-arboreal pollen in orange (Litt and Stebich, 1999; Litt et al., 2009; Litt and Stebich, 2001; Litt, 2025, 2001). Finally, Holzmaar pollen is in solid colour, whereas Meerfelder Maar pollen is underlaying the Holzmaar pollen and is transparent. The horizontal gray bar marks the stratigraphic position of the Laacher See Tephra (LST) and the stratigraphy is following Lang et al. (2023); Litt and Stebich (1999) with the exact age boundaries following Birlo et al. (2023).

https://doi.org/10.5194/egusphere-2026-1390
Preprint. Discussion started: 20 March 2026

4 Discussion

4.1 Development of vegetation

The pollen records from Meerfelder Maar (MFM) and Holzmaar (HZM) reveal a transformation of the catchment during the transition from the Pleniglacial to the Late Glacial (Fig. 3). The onset of the Bølling ($\sim 14,450$ cal yr BP) is marked by an increase in *Juniperus* concurrent with a relative decline in *Pinus*. Only in the late Bølling, the gradual establishment of *Betula* is observed.

At the onset of the Allerød, *Betula* became the dominant tree taxon in the catchment, although total Arboreal Pollen (AP) abundances remained below the closed forest threshold ($< 80\%$, Lang (1994); Sugita et al. (1999)). This expansion coincides stratigraphically with the onset of preservation of biochemical varves and the appearance of indicators of anoxia.

Progressing through the Allerød, the vegetation shifted from *Betula* to *Pinus*. The percentages of *Betula* pollen gradually declined, while *Pinus* pollen increased, eventually replacing *Betula* as the dominant tree species by the late Allerød. The termination of the anoxic phase (disappearance of okenone) at the onset of the Younger Dryas coincided with the decline of *Betula*. In contrast, regional AP values remained high ($\sim 70\%$, Litt and Stebich (1999)) due to the persistence of *Pinus*, indicating that the recovery of the lake's oxygenation state occurred despite sustained forest cover.

4.2 Succession of primary producers

The high-resolution pigment stratigraphy of Holzmaar reveals a distinct ecological succession that mirrors the primary producer succession in the lake, validating the use of hyperspectral imaging (HSI) for mapping phototrophic communities in varved sediments (Zander et al., 2023).

The Pioneer Community (Pleniglacial) corresponds to a generally mixed water column influenced by high detrital input (Ti). This signal reflects local loess deflation from the Rhine Valley, driven by high winds and limited vegetation cover, and cold mean annual temperatures (insolation, Fig. 4 and Fig. A3). The primary producer assemblage is dominated by benthic diatoms such as *Staurosira construens* (García et al., 2022; Lotter and Bigler, 2000) and generalist cyanobacteria (Fig. 3). Notably, the pigment assemblage (Fig. 2) is dominated by alloxanthin (Cryptophytes), characteristic of pioneer communities in glacial minerogenic sediments adapted to low-light conditions (Züllig, 1986). Further, the presence of isorenieratene indicates the existence of green sulphur bacteria (*Chlorobiaceae*). As these obligate anaerobes can tolerate extremely low light, their presence in this generally oxic phase suggests that they occupied stable, anoxic micro-niches, likely under seasonal ice cover or the sediment-water interface in the littoral zone. This community may be analogous to modern assemblages found in polar lakes (Antoniades et al., 2009) or the early developmental stages of Lake Jaczno (Makri et al., 2021), where the cryolittoral zone creates transient anoxic habitats.

The Secondary Colonizers (Early Bølling) reflect the immediate biological response to rapid climatic warming (Fig. 4, $\delta^{18}O_{NGRIP}$) and the onset of thermal stratification. This transition is marked by the expansion of the benthic/periphytic, mesotrophic diatom *Amphora indistincta*, replacing oligotrophic pioneer taxa. *Amphora indistincta* typically colonizes submerged macrophytes or mineral substrates in the littoral zone (Levkov, 2009). Its expansion, simultaneous with the sharp rise

https://doi.org/10.5194/egusphere-2026-1390
Preprint. Discussion started: 20 March 2026

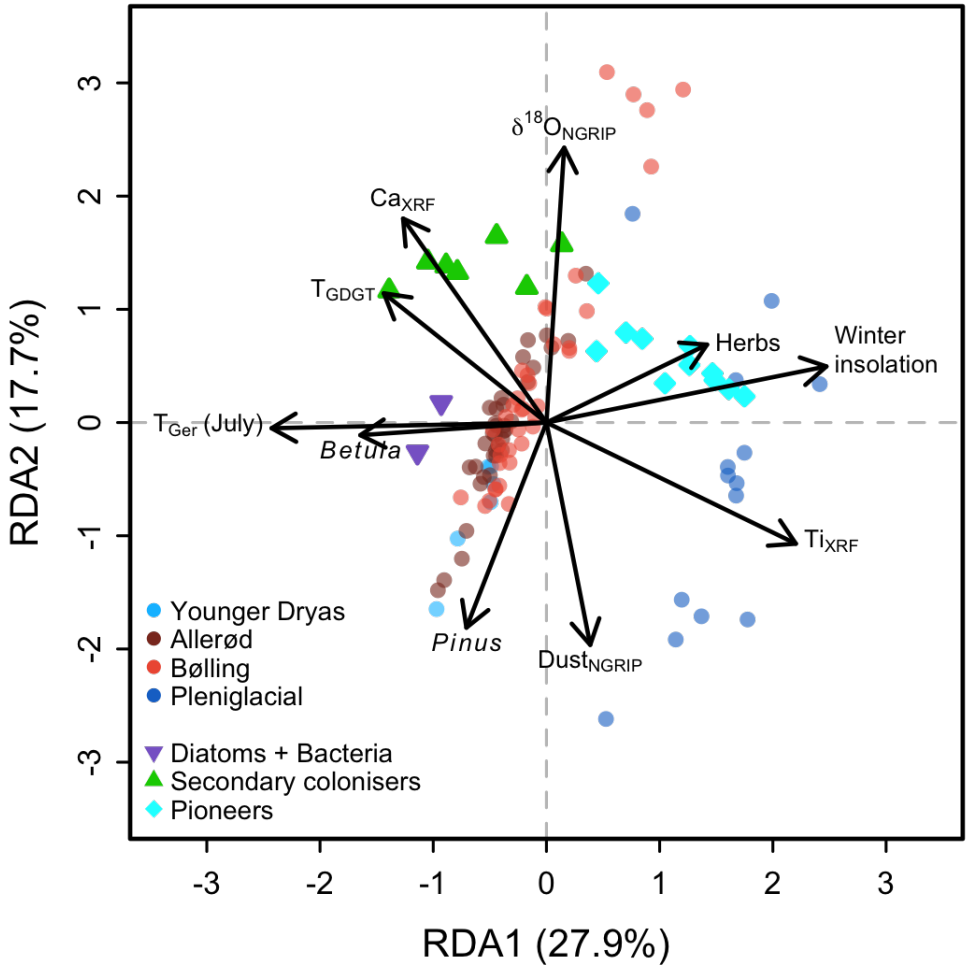

Figure 4. Redundancy Analysis (RDA) of sedimentary pigment assemblages and environmental drivers. The biplot displays the relationship between the primary producer community (pigments, response variables) and independent environmental proxies (explanatory variables). Individual samples are displayed as solid points, which are colour-coded according to their pollen zones. The identified pigments are colour-coded according to the three pigment groups assigned in Figure 2: Pioneer, Secondary Colonizers and Diatoms + Bacteria. Solid arrows represent the significant explanatory variables ($p < 0.05$), including catchment vegetation (*Betula*, *Pinus* pollen, non-arboreal pollen (Herbs)), regional temperature (NGRIP δ^{18}O) and dust ($\mathrm{Dust_{NGRIP}}$), GDGT-derived lake temperature ($\mathrm{T_{GDGT}}$), chironomid-based July temperature at Gerzensee, Switzerland ($\mathrm{T_{Ger}}$ July, (Lotter et al., 2012)), allochthonous minerogenic input ($\mathrm{Ti_{XRF}}$) and calcite ($\mathrm{Ca_{XRF}}$). The first two axes explain 27.9% and 17.7% of the total variance, respectively. The alignment of *Betula* and July temperature with the late-successional community (purple, nabla) highlights the link between climate, watershed vegetation expansion and the establishment of stable anoxic conditions.

in cyanobacterial pigments (Fig. 3), likely reflects a rising lake level and the creation of new littoral habitats (Negendank and Zolitschka, 1993). Further, the proliferation of the planktonic diatom *Stephanodiscus minutulus* (García et al., 2022) suggests

https://doi.org/10.5194/egusphere-2026-1390
Preprint. Discussion started: 20 March 2026

that despite the trend toward thermal stratification (occurrence of okenone), Holzmaar maintained a robust seasonal mixing regime (likely monomixis) that allowed nutrient regeneration and kept heavy diatoms in suspension.

During this period, the watershed was colonized by *Juniperus* (Fig. 3). As a light-demanding pioneer, its presence implies an open canopy structure before the establishment of forests. We propose that the interplay of rising lake levels (dilution) and developing littoral zones created dynamic niches that were rapidly filled by this secondary community. Geochemically, the gradual increase in bioavailable manganese (Mn F2+F3) confirms that these changes were accompanied by efficient Mn sequestration during oxic conditions linked to regular lake mixing.

The late successional lake community (Allerød) marks the transition to stable euxinia. The physical and chemical properties of the lake were heavily influenced by summer temperatures and establishment of *Betula* in the watershed (Fig. 4). The dominance of okenone (Fig. 3) signals that the chemocline reached into the photic zone. This pigment is specific to purple sulphur bacteria (PSB, *Chromatiaceae*) and indicates the formation of a dense, self-shading bacterial plate. This structure, comprising of purple sulphur bacteria (PSB, *Chromatiaceae*) and green sulphur bacteria (GSB, *Chlorobiaceae*), is analogous to the deep chlorophyll maxima observed in modern Lake Cadagno (Tonolla et al., 2005; Zander et al., 2023). The persistence of this community throughout the Allerød confirms that the lake entered a stable state of persistent anoxia or at least seasonally stratified settings, resilient to minor climate fluctuations, such as centennial-scale oscillations in warm-season temperatures, periodic shifts in humidity, and the short-lived cooling of the Intra-Allerød Cold Period (IACP) documented in the Eifel region (Zander et al., 2024; Litt and Stebich, 1999).

The co-occurrence of these anaerobic bacteria with oxic indicators (*Stephanodiscus minutulus*) presents an apparent paradox. While *S. minutulus* is traditionally interpreted as a signal of vigorous spring circulation (Kienel et al., 2017), its presence alongside PSB suggests a high degree of ecological plasticity. Rather than purely reflecting seasonal mixing, this co-existence likely highlights the ability of *S. minutulus* to thrive in low-light, and shaded environments (Fietz and Nicklisch, 2002; Gladyshev et al., 2010). Such adaptability allows these diatoms to maintain competitive strategies in light-limiting environments (Celewicz and Gołdyn, 2021; Estepp and Reavie, 2015).

In Holzmaar, this resilience enabled *S. minutulus* to thrive in the lower epilimnion immediately above the bacterial plate, despite the self-shading effects of the dense PSB community (Guasch and Subater, 1995; Köhler et al., 2017; Pestryakova et al., 2018). Based on this high-resolution HSI data, we propose two non-exclusive scenarios for this community structure: (1) Seasonal succession: A temporal separation where spring mixing supports diatom blooms, followed by stable summer stratification dominated by PSB. In this case, the low-light adaptation of *S. minutulus* would allow it to persist longer into the early stages of stratification as the chemocline rises. (2) Spatial co-existence: A Deep Chlorophyll Maximum (DCM) where diatoms thrive in the lower epilimnion immediately above the bacterial plate (Spanbauer et al., 2014). Our high-resolution HSI data support a dual mechanism: the HSI maps (Fig. 5) reveal a complex stratigraphy where layers containing both pigments (indicating simultaneous summer production) are interbedded with layers of exclusively PSB or chlorophylls (indicating strict seasonal separation).

https://doi.org/10.5194/egusphere-2026-1390
Preprint. Discussion started: 20 March 2026

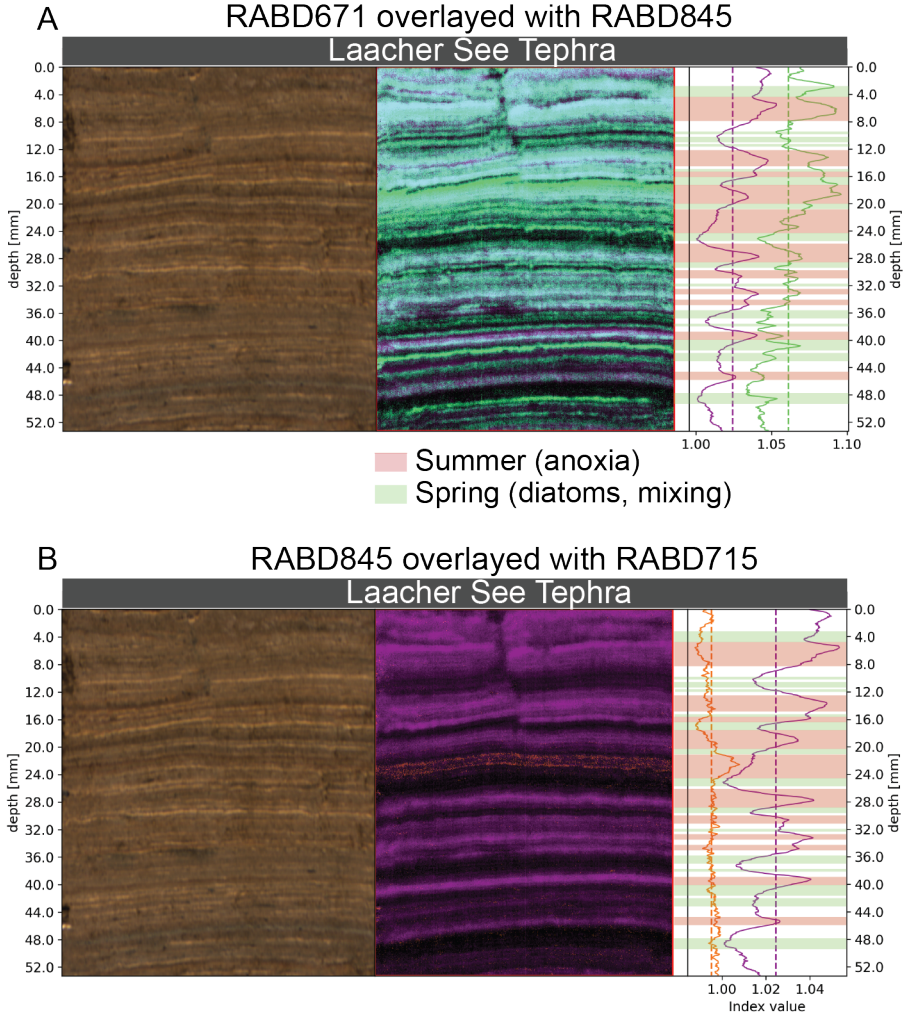

Figure 5. Selected section of core HZM19_11_7 from 65.2-70.5 cm (∼ 13,015-13,102 cal yr BP) demonstrating hyperspectral imaging data (HSI) of varves and pigment distributions represented by RABDs immediately below the LST. (A) Green colour and lines (RABD671) correspond to chlorophyll *a* derivatives (green algae/diatoms), while purple/pink colour and lines (RABD845) indicate bacteriopheophytin *a* (purple sulphur bacteria). (B) The same section as in panel A, where purple/pink colour and lines (RABD845) indicate bacteriopheophytin *a* (purple sulphur bacteria) and orange colour and lines (RABD715) show distribution of bacteriochlorophyll *e* (green sulphur bacteria). Both, the separation of layers as well as overlaps of the pigments are observed. Summer layers are highlighted in the plot area by red overlay and spring layers are highlighted in green. Dashed lines represent mean RABD values of the section.

4.3 Anoxia drivers

380 Disentangling the drivers of anoxia requires separating the regional temperature trends from local catchment forcing. While local warm-season temperatures increased moderately by $\sim +2.8°C$ in the period from 14,642 to 12,846 cal yr BP (Zander

https://doi.org/10.5194/egusphere-2026-1390
Preprint. Discussion started: 20 March 2026

et al., 2024), the primary driver of the presence of anoxia in the photic zone was likely the termination of extreme winter cooling (Bekaert et al., 2023). This shift prevented deep freezing and extended the thermal stratification period into warm-seasons, providing the physical boundary conditions for anoxia. However, the specific timing of the euxinic phase, which lags the initial warming, suggests an influence of catchment-mediated processes, such as vegetation and soil development, to cross the anoxia threshold.

In addition to regional climate, the onset of anoxia was likely pre-conditioned by the specific basin morphometry of Holzmaar. With a relative depth (Z_r, a ratio of maximum depth to lake mean diameter) of 7.4%, the volcanic maar basin is morphologically predisposed to stable thermal stratification by decoupling the hypolimnion from wind-driven mixing (Lehner, 2024; Magee and Wu, 2017). Global predictive models suggest that a high Z_r, combined with rising temperatures, moved the onset of spring stratification earlier in the season (Demers and Kalff, 1993). While direct evidence for lake-level fluctuations at Holzmaar is limited, regional records indicate higher lake levels during the Bølling-Allerød across Central Europe (Magny, 2001). Such a deepening would have increased Z_r and physically primed the system for anoxia. Within this physically sensitive framework, the expansion of *Betula* in the watershed acted as a reinforcing factor. However, given the high crater rim ($< +35$ m) and significant relative depth (-20 m), the threshold of arboreal pollen (AP) required to shield the lake from wind was likely much lower than in shallower basins. This implies that the lake was physically predisposed to stability regardless of subtle changes in forest density.

The onset of intense anoxia coincides precisely with the expansion of *Betula* in the watershed and a reduction in allochthonous sediment yield (from 16 to $< 2\,\mathrm{t \cdot km^{-2} \cdot yr^{-1}}$), as quantified by Zolitschka (1998). This confirms that vegetation stabilized the crater slopes and its catchment. We propose that *Betula* afforestation employed a dual control on the lake physics: (1) Wind shielding: The forestation of the crater rim likely acted as a roughness filter, dampening the windshear required for deep mixing (Dietrich and Seelos, 2010; Makri et al., 2020; Zander et al., 2021b; Wienhues et al., 2026). (2) Chemical coupling: Unlike eroding minerogenic matter during the Pleniglacial, the developing organic soils under *Betula* vegetation likely increased the export of Dissolved Organic Carbon (DOC). While we lack direct DOC reconstructions, the shift to organic sedimentation implies a change in light penetration and heat absorption, a mechanism known to enhance thermal stability in small lakes (Meyer-Jacob et al., 2019).

At Holzmaar, anoxia disappeared precisely at the onset of the Younger Dryas (YD), although *Pinus* coverage increased (Fig. 6). This recovery highlights that climatic cooling and a regional shift towards less humid conditions were the decisive drivers for breaking stable lake stratification. The temperature decline and increased aridity overrode the physical shielding of the crater rim by increasing water density and enhancing convective mixing. Consequently, the shift in forest composition (from *Betula* to *Pinus*) is interpreted as a climatically-driven consequence rather than the main cause of re-oxygenation.

While vegetation shifts occur slower than physical changes in lake mixing, the change in forest composition may have provided a secondary, stabilizing feedback. *Betula* produces labile, sugar-rich leaves that decompose rapidly, exerting a high biological oxygen demand that maintains anoxia. In contrast, the shift to *Pinus* introduced recalcitrant, lignin-rich needles, which are slower to degrade, effectively reducing microbial respiration rates and allowing the water column to re-oxygenate despite continued forest cover (Sobek et al., 2007; Catalán et al., 2016). Thus, while the shift of the OM source influenced

https://doi.org/10.5194/egusphere-2026-1390
Preprint. Discussion started: 20 March 2026

the resilience of the anoxic state, the initial transition was triggered by the cold and arid climatic forcing of the Younger Dryas, a transition clearly reflected in the stratigraphic trajectory of pigment assemblages, which exhibits a return toward the pioneer-community space (Fig. A5).

4.4 Geochemical buffering and ecosystem resilience

The geochemical response of Holzmaar reveals a highly efficient nutrient retention mechanism that distinguishes it from purely iron-controlled (Søndergaard et al., 2003; Gächter and Müller, 2003) or carbonate-controlled lakes (Tu et al., 2020). Within the reactive pool (Fraction 2), the molar Fe:P ratio stabilizes at ~ 1.5 throughout the anoxic phase (Fig. A6). This stoichiometry is the diagnostic signature of formation of authigenic ferrous phosphates such as vivianite ($Fe_3(PO_4)_2 \cdot 8H_2O$) in iron-rich sediments (Nriagu, 1972; Rothe et al., 2016; Kleeberg et al., 2013). It indicates that the volcanic iron flux (Förster et al., 2019) provided a sufficient reactive buffer to sequester phosphorus in the sediment throughout the DOE-1, even under reducing conditions (O'Connell et al., 2015).

The sequential extraction data further identify the acid-soluble Fraction 4 (HCl, Fig. A6) as the dominant long-term sink for manganese, iron, and phosphorus. We interpret this stable pool as the result of a dual-retention mechanism: initially, the reactive iron pool (F2) traps porewater phosphorus as vivianite (($Fe_3(PO_4)_2 \cdot 8H_2O$), and subsequently, this phosphorus is buried within or converted into stable mineral phases in Fraction 4 that do not redissolve during redox shifts. By permanently locking P, Mn and Fe into this stable sink, the lake avoided the development of a chemical legacy or an internal phosphorus loading (Søndergaard et al., 2003). The biological consequence of this geochemical resilience is a high degree of community reversibility, as the pigment assemblages effectively return to the pioneer-community once the climatic drivers of the Allerød (warming) were removed (Fig. A5).

This geochemical framework provides critical insight into lake ecosystem resilience and rapid high reversibility. We attribute this resilience to a specific decoupling of nutrient cycles under an iron-unlimited regime. While manganese followed the expected reductive dissolution-precipitation pattern, being recycled back into the water column during anoxia (depleted F2) and precipitated during the seasonal mixing (increase F2+3), phosphorus behaved differently. In many eutrophic or carbonate-dominated systems, such as Lake Burgäschi, Lake Baldeggersee or Lake Soppensee (Swiss Plateau, Tu et al. (2020); Lotter (1998); Schouten et al. (2026), the release of legacy phosphorus creates a delayed recovery, sustaining anoxia long after external climate forcings are removed (Carpenter, 2005; Søndergaard et al., 2003). In those systems, sulfate reduction often strips iron from the sediments to form minerals like pyrite, releasing phosphorus back into the water column (Tu et al., 2020; Lotter, 1998; Schouten et al., 2026).

Consequently, regional cooling at the onset of the Younger Dryas allowed the system to re-oxygenate, evidenced by the decline of anoxia followed by the vegetation shift (*Betula* to *Pinus*) with a minimal time lag (Fig. 6). This recovery may have been further facilitated by the shift from labile *Betula* vegetation to recalcitrant *Pinus* forest, which potentially reduced microbial oxygen demand (Sobek et al., 2007; Catalán et al., 2016). Ultimately, while climate and vegetation set the boundary conditions, the specific coupling of catchment characteristics and an iron-rich lithogenic buffer determined the resilience of the aquatic ecosystem.

https://doi.org/10.5194/egusphere-2026-1390
Preprint. Discussion started: 20 March 2026

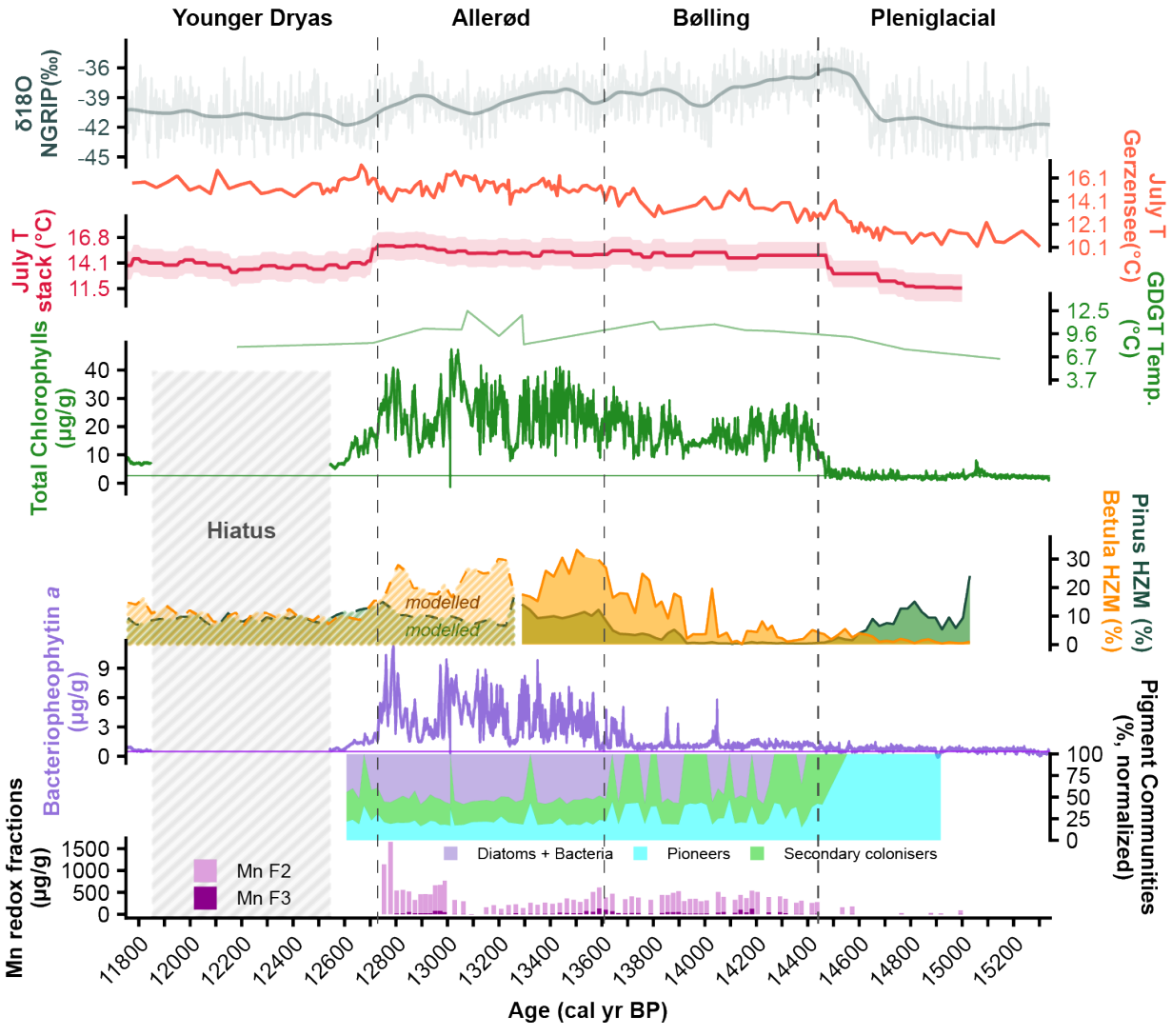

Figure 6. Multi-proxy summary of climatic, vegetational, and geochemical transitions at Holzmaar. The top panels display (from top to bottom): NGRIP $\delta^{18}O$ and regional temperature reconstructions, including Gerzensee July T, the Alpine July T stack, and local GDGT-derived temperatures (T_{GDGT}). Mid-panels show total chlorophyll concentrations (a proxy for primary production) and *Betula* and *Pinus* pollen percentages (with modeled sections indicated). Lower panels illustrate the concentrations of the anoxia indicator bacteriopheophytin *a* (unsmoothed) alongside the relative abundance of phototrophic pigment communities (Pioneers, Secondary Colonizers, and Diatoms + Bacteria). The bottom panel presents reactive manganese (Mn) redox fractions F2 and F3. Vertical dashed lines delineate the major biozones. Data sources: NGRIP (NGRIP Members, 2004), Gerzensee July T (Lotter et al., 2012), July T stack (Heiri et al., 2014), T_{GDGT} (Zander et al., 2024), HZM *Betula* pollen (Litt, 2010, 2001).

https://doi.org/10.5194/egusphere-2026-1390
Preprint. Discussion started: 20 March 2026

5 Conclusions

This study reconstructs the high-resolution biological and geochemical responses of a volcanic maar lake to rapid natural warming (DOE-1), providing a mechanistic template for understanding climate-driven anoxia without anthropogenic interference.

We demonstrate that hyperspectral imaging can resolve micro-stratigraphic shifts in phototrophic communities within varved sediments. The succession at Holzmaar progressed from an oligotrophic, pioneer community to a late-successional stage where the chemocline reached into the photic zone. This allowed purple sulphur bacteria to thrive alongside oxic low-light adapted planktonic diatom (*Stephanodiscus minutulus*), creating a complex biological structure analogous to modern meromictic systems where primary production is maintained across steep light and redox gradients.

Further, our multi-proxy approach reveals that atmospheric warming was a necessary driver for sustained anoxia, though its impact was modulated by local factors. The onset of stratification was likely pre-conditioned by the lake's high relative depth ($Z_r = 7.4\%$), a physical state that may have been amplified by climate-driven increases in lake level. Within this physically sensitive framework, the stabilization of catchment soils by *Betula* and the associated export of organic matter acted as a reinforcing factor for lake stratification. The rapid recovery of the lake was triggered primarily by the onset of the Younger Dryas cooling and increased aridity, which has physically broken the stable stratification. This transition caused changes in catchment vegetation including the shift from *Betula* to *Pinus*, which may have provided a secondary feedback by reducing microbial oxygen demand.

Finally, we identify a distinct lithological control on ecosystem resilience. Unlike carbonate-dominated systems that often suffer from internal phosphorus loading (hysteresis), Holzmaar functioned as an efficient nutrient trap. The volcanic catchment provided a continuous flux of reactive iron that prevented the release of phosphorus via reductive dissolution by sequestering it into stable mineral phases. Due to the absence of this positive biogeochemical feedback, the biological community reverted to an oxygenated state immediately upon the onset of climatic cooling and drying.

These findings suggest that while climate warming sets the physical potential for anoxia, the vulnerability and recovery of lake ecosystems are driven by the specific coupling between temperature, regional moisture balance, catchment vegetation, and their lithogenic redox buffer.

Code and data availability. The code for the data processing, statistical analysis and plotting is available at https://github.com/Epta13/Holzmaar2022-2025.git and readily executable at https://renkulab.io/p/snsf-anoxia-project/holzmaar. All the data used in this publication are available at https://doi.org/10.5281/zenodo.18429717.

Author contributions. PZ – Conceptualisation, Methodology, Formal analysis, Investigation, Visualisation, Data Curation, Software, Writing - Original Draft, MLG – Formal analysis, Investigation, Writing - Review & Editing, SB - Formal analysis, Investigation, Writing - Review & Editing, AL - Formal analysis, Investigation, Writing - Review & Editing, MS - Formal analysis, Investigation, Writing - Review & Editing,

https://doi.org/10.5194/egusphere-2026-1390
Preprint. Discussion started: 20 March 2026

SJS - Writing - Review & Editing, NRMMS – Writing - Review & Editing, BZ - Resources, Writing - Review & Editing, HV - Methodology, Writing - Review & Editing, MG - Conceptualisation, Resources, Supervision, Funding acquisition, Writing - Review & Editing

Competing interests. Authors declare no competing interests.

485 *Acknowledgements.* This works was supported by Swiss National Science Foundation 200020_204220.

https://doi.org/10.5194/egusphere-2026-1390
Preprint. Discussion started: 20 March 2026

References

Aitchison, J.: The Statistical Analysis of Compositional Data, Journal of the Royal Statistical Society Series B: Statistical Methodology, 44, 139–160, https://doi.org/10.1111/j.2517-6161.1982.tb01195.x, 1982.

Albrecht, M., Ruther, A., and Sandmann, G.: Purification and biochemical characterization of a hydroxyneurosporene desaturase involved in the biosynthetic pathway of the carotenoid spheroidene in Rhodobacter sphaeroides, Journal of Bacteriology, 179, 7462–7467, https://doi.org/10.1128/jb.179.23.7462-7467.1997, 1997.

Antoniades, D., Veillette, J., Martineau, M.-J., Belzile, C., Tomkins, J., Pienitz, R., Lamoureux, S., and Vincent, W. F.: Bacterial dominance of phototrophic communities in a High Arctic lake and its implications for paleoclimate analysis, Polar Science, 3, 147–161, https://doi.org/10.1016/j.polar.2009.05.002, 2009.

Bekaert, D., Blard, P.-H., Raoult, Y., Pik, R., Kipfer, R., Seltzer, A., Legrain, E., and Marty, B.: Last glacial maximum cooling of 9 °C in continental Europe from a 40 kyr-long noble gas paleothermometry record, Quaternary Science Reviews, 310, 108 123, https://doi.org/10.1016/j.quascirev.2023.108123, 2023.

Bertrand, M.: Carotenoid biosynthesis in diatoms, Photosynthesis Research, 106, 89–102, https://doi.org/10.1007/s11120-010-9589-x, 2010.

Bertrand, S., Tjallingii, R., Kylander, M. E., Wilhelm, B., Roberts, S. J., Arnaud, F., Brown, E., and Bindler, R.: Inorganic geochemistry of lake sediments: A review of analytical techniques and guidelines for data interpretation, Earth-Science Reviews, 249, 104 639, https://doi.org/10.1016/j.earscirev.2023.104639, 2024.

Bianchi, T. S. and Canuel, E. A.: Chemical Biomarkers in Aquatic Ecosystems, https://doi.org/10.1515/9781400839100, 2011.

Biebl, H. and Pfennig, N.: Growth yields of green sulfur bacteria in mixed cultures with sulfur and sulfate reducing bacteria, Archives of Microbiology, 117, 9–16, https://doi.org/10.1007/BF00689344, 1978.

Birlo, S., Tylmann, W., and Zolitschka, B.: Bayesian age–depth modelling applied to varve and radiometric dating to optimize the transfer of an existing high-resolution chronology to a new composite sediment profile from Holzmaar (West Eifel Volcanic Field, Germany), Geochronology, 5, 65–90, https://doi.org/10.5194/gchron-5-65-2023, 2023.

Brauer, A., Litt, T., Negendank, J. F., and Zolitschka, B.: Lateglacial varve chronology and biostratigraphy of lakes Holzmaar and Meerfelder Maar, Germany, Boreas, 30, 83–88, https://doi.org/10.1111/j.1502-3885.2001.tb00991.x, 2001.

Butz, C., Grosjean, M., Fischer, D., Wunderle, S., Tylmann, W., and Rein, B.: Hyperspectral imaging spectroscopy: a promising method for the biogeochemical analysis of lake sediments, Journal of Applied Remote Sensing, 9, 096 031–096 031, https://doi.org/10.1117/1.jrs.9.096031, publisher: Society of Photo-Optical Instrumentation Engineers, 2015.

Butz, C., Grosjean, M., Goslar, T., and Tylmann, W.: Hyperspectral imaging of sedimentary bacterial pigments: a 1700-year history of meromixis from varved Lake Jaczno, northeast Poland, Journal of Paleolimnology, 58, 57–72, https://doi.org/10.1007/s10933-017-9955-1, 2017.

Carpenter, S. R.: Eutrophication of aquatic ecosystems: Bistability and soil phosphorus, Proceedings of the National Academy of Sciences, 102, 10 002–10 005, https://doi.org/10.1073/pnas.0503959102, 2005.

Catalán, N., Marcé, R., Kothawala, D. N., and Tranvik, L. J.: Organic carbon decomposition rates controlled by water retention time across inland waters, Nature Geoscience, 9, 501–504, https://doi.org/10.1038/ngeo2720, 2016.

Celewicz, S. and Gołdyn, B.: Phytoplankton communities in temporary ponds under different climate scenarios, Scientific Reports, 11, https://doi.org/10.1038/s41598-021-97516-9, 2021.

https://doi.org/10.5194/egusphere-2026-1390
Preprint. Discussion started: 20 March 2026

Chen, N., Bianchi, T. S., McKee, B. A., and Bland, J. M.: Historical trends of hypoxia on the Louisiana shelf: application of pigments as biomarkers, Organic Geochemistry, 32, 543–561, https://doi.org/10.1016/S0146-6380(00)00194-7, 2001.

Coolen, M. J. L. and Overmann, J.: Analysis of Subfossil Molecular Remains of Purple Sulfur Bacteria in a Lake Sediment, Applied and Environmental Microbiology, 64, 4513–4521, https://doi.org/10.1128/aem.64.11.4513-4521.1998, 1998.

Davies, B. H., Holmes, E. A., Loeber, D. E., Toube, T. P., and Weedon, B. C. L.: Carotenoids and related compounds. Part XXIII. Occurrence of 7,8,11,12-tetrahydrolycopene, spheroidene, 3,4,11′,12′-tetrahydrospheroidene, and 11′,12′-dihydrospheroidene in Rhodospirillum rubrum, J. Chem. Soc. C, 0, 1266–1268, https://doi.org/10.1039/J39690001266, 1969.

Demers, E. and Kalff, J.: A simple model for predicting the date of spring stratification in temperate and subtropical lakes, Limnology and Oceanography, 38, 1077–1081, https://doi.org/10.4319/lo.1993.38.5.1077, 1993.

Deshpande, B. N., Tremblay, R., Pienitz, R., and Vincent, W. F.: Sedimentary pigments as indicators of cyanobacterial dynamics in a hypereutrophic lake, Journal of Paleolimnology, 52, 171–184, https://doi.org/10.1007/s10933-014-9785-3, 2014.

Dietrich, S. and Seelos, K.: The reconstruction of easterly wind directions for the Eifel region (Central Europe) during the period 40.3–12.9 ka BP, Climate of the Past, 6, 145–154, https://doi.org/10.5194/cp-6-145-2010, 2010.

Estepp, L. R. and Reavie, E. D.: The ecological history of Lake Ontario according to phytoplankton, Journal of Great Lakes Research, 41, 669–687, https://doi.org/10.1016/j.jglr.2015.06.005, 2015.

Fiedor, J., Fiedor, L., Kammhuber, N., Scherz, A., and Scheer, H.: Photodynamics of the Bacteriochlorophyll–Carotenoid System. 2. Influence of Central Metal, Solvent andβ-Carotene on Photobleaching of Bacteriochlorophyll Derivatives, Photochemistry and Photobiology, 76, 145, https://doi.org/10.1562/0031-8655(2002)076<0145:potbcs>2.0.co;2, 2002.

Fietz, S. and Nicklisch, A.: Acclimation of the diatom Stephanodiscus neoastraea and the cyanobacterium Planktothrix agardhii to simulated natural light fluctuations, Photosynthesis Research, 72, 95–106, https://doi.org/10.1023/A:1016052726149, 2002.

Förster, M. W., Zemlitskaya, A., Otter, L. M., Buhre, S., and Sirocko, F.: Late Pleistocene Eifel eruptions: insights from clinopyroxene and glass geochemistry of tephra layers from Eifel Laminated Sediment Archive sediment cores, Journal of Quaternary Science, 35, 186–198, https://doi.org/10.1002/jqs.3134, 2019.

García, M. L., Birlo, S., and Zolitschka, B.: Paleoenvironmental changes of the last 16,000 years based on diatom and geochemical stratigraphies from the varved sediment of Holzmaar (West-Eifel Volcanic Field, Germany), Quaternary Science Reviews, 293, 107 691, https://doi.org/10.1016/j.quascirev.2022.107691, 2022.

Gkinis, V., Simonsen, S., Buchardt, S., White, J., and Vinther, B.: Water isotope diffusion rates from the NorthGRIP ice core for the last 16,000 years – Glaciological and paleoclimatic implications, Earth and Planetary Science Letters, 405, 132–141, https://doi.org/10.1016/j.epsl.2014.08.022, 2014.

Gladyshev, M. I., Sushchik, N. N., Makhutova, O. N., Dubovskaya, O. P., Kravchuk, E. S., Kalachova, G. S., and Khromechek, E. B.: Correlations between fatty acid composition of seston and zooplankton and effects of environmental parameters in a eutrophic Siberian reservoir, Limnologica, 40, 343–357, https://doi.org/10.1016/j.limno.2009.12.004, 2010.

Glaeser, J., Bañeras, L., Rütters, H., and Overmann, J.: Novel bacteriochlorophyll e structures and species-specific variability of pigment composition in green sulfur bacteria, Archives of Microbiology, 177, 475–485, https://doi.org/10.1007/s00203-002-0416-4, 2002.

Guasch, H. and Subater, S.: SEASONAL VARIATIONS IN PHOTOSYNTHESIS-IRRADIANCE RESPONSES BY BIOFILMS IN MEDITERRANEAN STREAMS, Journal of Phycology, 31, 727–735, https://doi.org/10.1111/j.0022-3646.1995.00727.x, 1995.

Guilizzoni, P. and Lami, A.: Paleolimnology: Use of Algal Pigments as Indicators, in: Encyclopedia of Environmental Microbiology, edited by Bitton, G., Wiley, ISBN 9780471263395, https://doi.org/10.1002/0471263397.env313, 2003.

https://doi.org/10.5194/egusphere-2026-1390
Preprint. Discussion started: 20 March 2026

Gächter, R. and Müller, B.: Why the phosphorus retention of lakes does not necessarily depend on the oxygen supply to their sediment surface, Limnology and Oceanography, 48, 929–933, https://doi.org/10.4319/lo.2003.48.2.0929, 2003.

Heiri, O., Ilyashuk, B., Millet, L., Samartin, S., and Lotter, A. F.: Stacking of discontinuous regional palaeoclimate records: Chironomid-based summer temperatures from the Alpine region, The Holocene, 25, 137–149, https://doi.org/10.1177/0959683614556382, 2014.

Jeffrey, S. t. and Humphrey, G.: New spectrophotometric equations for determining chlorophylls a, b, c1 and c2 in higher plants, algae and natural phytoplankton, Biochemie und physiologie der pflanzen, 167, 191–194, https://doi.org/10.1016/s0015-3796(17)30778-3, 1975.

Jenny, J., Francus, P., Normandeau, A., Lapointe, F., Perga, M., Ojala, A., Schimmelmann, A., and Zolitschka, B.: Global spread of hypoxia in freshwater ecosystems during the last three centuries is caused by rising local human pressure, Global Change Biology, 22, 1481–1489, https://doi.org/10.1111/gcb.13193, 2016.

Jensen, H. S., Kristensen, P., Jeppesen, E., and Skytthe, A.: Iron:phosphorus ratio in surface sediment as an indicator of phosphate release from aerobic sediments in shallow lakes, Hydrobiologia, 235, 731–743, https://doi.org/10.1007/978-94-011-2783-7_66, 1992.

Kaufman, D., McKay, N., Routson, C., Erb, M., Davis, B., Heiri, O., Jaccard, S., Tierney, J., Dätwyler, C., Axford, Y., Brussel, T., Cartapanis, O., Chase, B., Dawson, A., de Vernal, A., Engels, S., Jonkers, L., Marsicek, J., Moffa-Sánchez, P., Morrill, C., Orsi, A., Rehfeld, K., Saunders, K., Sommer, P. S., Thomas, E., Tonello, M., Tóth, M., Vachula, R., Andreev, A., Bertrand, S., Biskaborn, B., Bringué, M., Brooks, S., Caniupán, M., Chevalier, M., Cwynar, L., Emile-Geay, J., Fegyveresi, J., Feurdean, A., Finsinger, W., Fortin, M.-C., Foster, L., Fox, M., Gajewski, K., Grosjean, M., Hausmann, S., Heinrichs, M., Holmes, N., Ilyashuk, B., Ilyashuk, E., Juggins, S., Khider, D., Koinig, K., Langdon, P., Larocque-Tobler, I., Li, J., Lotter, A., Luoto, T., Mackay, A., Magyari, E., Malevich, S., Mark, B., Massaferro, J., Montade, V., Nazarova, L., Novenko, E., Pařil, P., Pearson, E., Peros, M., Pienitz, R., Płóciennik, M., Porinchu, D., Potito, A., Rees, A., Reinemann, S., Roberts, S., Rolland, N., Salonen, S., Self, A., Seppä, H., Shala, S., St-Jacques, J.-M., Stenni, B., Syrykh, L., Tarrats, P., Taylor, K., van den Bos, V., Velle, G., Wahl, E., Walker, I., Wilmshurst, J., Zhang, E., and Zhilich, S.: A global database of Holocene paleotemperature records, Scientific Data, 7, https://doi.org/10.1038/s41597-020-0445-3, 2020.

Kienel, U., Kirillin, G., Brademann, B., Plessen, B., Lampe, R., and Brauer, A.: Effects of spring warming and mixing duration on diatom deposition in deep Tiefer See, NE Germany, Journal of Paleolimnology, 57, 37–49, https://doi.org/10.1007/s10933-016-9925-z, 2017.

Kleeberg, A., Herzog, C., and Hupfer, M.: Redox sensitivity of iron in phosphorus binding does not impede lake restoration, Water Research, 47, 1491–1502, https://doi.org/10.1016/j.watres.2012.12.014, 2013.

Köhler, J., Wang, L., Guislain, A., and Shatwell, T.: Influence of vertical mixing on light-dependency of phytoplankton growth, Limnology and Oceanography, 63, 1156–1167, https://doi.org/10.1002/lno.10761, 2017.

Lami, A., Niessen, F., Guilizzoni, P., Masaferro, J., and Belis, C. A.: Palaeolimnological studies of the eutrophication of volcanic Lake Albano (Central Italy), Journal of Paleolimnology, 10, 181–197, https://doi.org/10.1007/BF00684032, 1994.

Lami, A., Guilizzoni, P., and Marchetto, A.: High resolution analysis of fossil pigments, carbon, nitrogen and sulphur in the sediment of eight European Alpine lakes: the MOLAR project, Journal of Limnology, 59, https://doi.org/10.4081/jlimnol.2000.s1.15, 2000.

Lang, G.: Quartare Vegetationsgeschichte Europas: Methoden und Ergebnisse, vol. 27, Gustav Fischer Verlag, Jena, ISBN 978-3334604052, 1994.

Lang, G., Tinner, W., Morales-Molino, C., Schwörer, C., and Ammann, B.: Quaternary Vegetation Dynamics of Europe, chap. 4.1 Stratigraphies and chronological subdivisions of the Late-Glacial and the Holocene, pp. 137–144, Haupt, 2023.

Larocque-Tobler, I., Heiri, O., and Wehrli, M.: Late Glacial and Holocene temperature changes at Egelsee, Switzerland, reconstructed using subfossil chironomids, Journal of Paleolimnology, 43, 649–666, https://doi.org/10.1007/s10933-009-9358-z, 2009.

https://doi.org/10.5194/egusphere-2026-1390
Preprint. Discussion started: 20 March 2026

Laskar, J., Robutel, P., Joutel, F., Gastineau, M., Correia, A. C., and Levrard, B.: A long-term numerical solution for the insolation quantities of the Earth, Astronomy & Astrophysics, 428, 261–285, https://doi.org/10.1051/0004-6361:20041335, 2004.

Leavitt, P. R. and Hodgson, D. A.: Sedimentary Pigments, pp. 295–325, Springer Netherlands, Dordrecht, ISBN 9780306476686, https://doi.org/10.1007/0-306-47668-1_15, 2002.

Lehner, B.: Rivers and Lakes—Their Distribution, Origins, and Forms, chap. 4. Rivers and Lakes - Their Distribution, Origins and Forms, pp. 25–56, Academic Press, San Diego, 3rd edn., ISBN 9780128227015, https://doi.org/10.1016/b978-0-12-822701-5.00004-5, 2024.

Levkov, Z.: Amphora sensu lato, vol. 5 of *Diatoms of Europe*, A.R.G. Gantner Verlag K.G., Ruggell, ISBN 978-3-906166-70-4, 2009.

Litt, T.: Pollen counts of sediment core HZM from Holzmaar, PANGAEA data repository, https://doi.org/10.1594/PANGAEA.59879, 2001.

Litt, T.: Pollen profile THZM4AB, Holzmaar, Germany, https://doi.org/10.1594/PANGAEA.739893, 2010.

Litt, T.: Holzmaar pollen dataset, https://doi.org/10.21233/8zpk-nz51, brauer, A., T. Litt, J.F.W. Negendank, and B. Zolitschka. 2001. Lateglacial varve chronology and biostratigraphy of lakes Holzmaar and Meerfelder Maar, Germany. Boreas 30:83-88.Litt, T., and M. Stebich. 1999. Bio- and chronostratigraphy of the lateglacial in the Eifel region, Germany. Quaternary International 61:5-16.Litt, T., C. Schölzel, N. Kühl, and A. Brauer. 2009. Vegetation and climate history in the Westeifel Volcanic Field (Germany) during the past 11 000 years based on annually laminated lacustrine maar sediments. Boreas 38:679-690.Litt, T., M. Früchtl, B. Kubitz, and M. Stebich. 1997. Jungquartäre Floren in den Eifelmaaren. Terra Nostra 1997(7):54-62. Notes: Exkursionsführer zur 67. Jahrestagung der Paläontologischen GesellschaftLitt, T., M. Früchtl, B. Kubitz, and M. Stebich. 1997. Palaeobotanical investigations. Terra Nostra 1997(8):25-29. Notes: In: 7th International Symposium on Palaeolimnology, Excursion Guide Excursion B (Laacher See and Eifel Maar lakes), 2025.

Litt, T. and Stebich, M.: Bio-and chronostratigraphy of the lateglacial in the Eifel region, Germany, Quaternary International, 61, 5–16, https://doi.org/10.1016/s1040-6182(99)00013-0, 1999.

Litt, T. and Stebich, M.: Pollen counts of sediment core MFM6, https://doi.org/10.1594/PANGAEA.59877, 2001.

Litt, T., Schölzel, C., Kühl, N., and Brauer, A.: Vegetation and climate history in the Westeifel Volcanic Field (Germany) during the past 11 000 years based on annually laminated lacustrine maar sediments, Boreas, 38, 679–690, https://doi.org/10.1111/j.1502-3885.2009.00096.x, 2009.

Lone, A. M. and Balakrishna, K.: Deep and Frozen: High-Mountain Lakes as Sentinels of Regional Limnology and Global Environmental Changes, Limnology and Oceanography Bulletin, 32, 98–101, https://doi.org/10.1002/lob.10559, 2023.

Lotter, A. F.: The recent eutrophication of Baldeggersee (Switzerland) as assessed by fossil diatom assemblages, The Holocene, 8, 395–405, https://doi.org/10.1191/095968398674589725, 1998.

Lotter, A. F.: The palaeolimnology of Soppensee (Central Switzerlabnd), as evidenced by diatom, pollen, and fossil-pigment analyses, Journal of Paleolimnology, 25, 65–79, https://doi.org/10.1023/a:1008140122230, 2001.

Lotter, A. F. and Bigler, C.: Do diatoms in the Swiss Alps reflect the length of ice-cover?, Aquatic sciences, 62, 125, https://doi.org/10.1007/s000270050002, 2000.

Lotter, A. F. and Kienast, F.: Validation of a forest succession model by means of annually laminated sediments, 1992.

Lotter, A. F., Heiri, O., Brooks, S., van Leeuwen, J. F., Eicher, U., and Ammann, B.: Rapid summer temperature changes during Termination 1a: high-resolution multi-proxy climate reconstructions from Gerzensee (Switzerland), Quaternary Science Reviews, 36, 103–113, https://doi.org/10.1016/j.quascirev.2010.06.022, 2012.

Lottermoser, B., Schütz, U., Boenecke, J., Oberhänsli, R., Zolitschka, B., and Negendank, J. F.: Natural and anthropogenic influences on the geochemistry of Quaternary lake sediments from Holzmaar, Germany, Environmental Geology, 31, 236–247, https://doi.org/10.1007/s002540050185, 1997.

https://doi.org/10.5194/egusphere-2026-1390
Preprint. Discussion started: 20 March 2026

Lücke, A., Schleser, G. H., Zolitschka, B., and Negendank, J. F.: A Lateglacial and Holocene organic carbon isotope record of lacustrine palaeoproductivity and climatic change derived from varved lake sediments of Lake Holzmaar, Germany, Quaternary Science Reviews, 22, 569–580, https://doi.org/10.1016/s0277-3791(02)00187-7, 2003.

Lukkari, K., Hartikainen, H., and Leivuori, M.: Fractionation of sediment phosphorus revisited. I: Fractionation steps and their biogeochemical basis, Limnology and Oceanography: Methods, 5, 433–444, https://doi.org/10.4319/lom.2007.5.433, 2007.

Magee, M. R. and Wu, C. H.: Response of water temperatures and stratification to changing climate in three lakes with different morphometry, Hydrology and Earth System Sciences, 21, 6253–6274, https://doi.org/10.5194/hess-21-6253-2017, 2017.

Magny, M.: Palaeohydrological changes as reflected by lake-level fluctuations in the Swiss Plateau, the Jura Mountains and the northern French Pre-Alps during the Last Glacial–Holocene transition: a regional synthesis, Global and Planetary Change, 30, 85–101, https://doi.org/10.1016/s0921-8181(01)00080-7, 2001.

Makri, S., Lami, A., Lods-Crozet, B., and Loizeau, J.-L.: Reconstruction of trophic state shifts over the past 90 years in a eutrophicated lake in western Switzerland, inferred from the sedimentary record of photosynthetic pigments, Journal of Paleolimnology, 61, 129–145, https://doi.org/10.1007/s10933-018-0049-5, 2018.

Makri, S., Rey, F., Gobet, E., Gilli, A., Tinner, W., and Grosjean, M.: Early human impact in a 15,000-year high-resolution hyperspectral imaging record of paleoproduction and anoxia from a varved lake in Switzerland, Quaternary Science Reviews, 239, 106 335, https://doi.org/10.1016/j.quascirev.2020.106335, publisher: Elsevier, 2020.

Makri, S., Lami, A., Tu, L., Tylmann, W., Vogel, H., and Grosjean, M.: Holocene phototrophic community and anoxia dynamics in meromictic Lake Jaczno (NE Poland) using high-resolution hyperspectral imaging and HPLC data, Biogeosciences, 18, 1839–1856, https://doi.org/10.5194/bg-18-1839-2021, 2021.

Meyer-Jacob, C., Michelutti, N., Paterson, A. M., Cumming, B. F., Keller, W., and Smol, J. P.: The browning and re-browning of lakes: Divergent lake-water organic carbon trends linked to acid deposition and climate change, Scientific Reports, 9, 16 676, https://doi.org/10.1038/s41598-019-52912-0, 2019.

Negendank, J. F. and Zolitschka, B.: Maars and maar lakes of the Westeifel Volcanic Field, in: Paleolimnology of European maar lakes, pp. 61–80, Springer, 1993.

NGRIP Members: High-resolution record of Northern Hemisphere climate extending into the last interglacial period, Nature, 431, 147–151, https://doi.org/10.1038/nature02805, 2004.

Nriagu, J. O.: Stability of vivianite and ion-pair formation in the system Fe3 (PO4) 2-H3PO4-H2O, Geochim Cosmochim Acta, 36, 459–470, https://doi.org/10.1016/0016-7037(72)90035-x, 1972.

Oelze, J.: 9 Analysis of Bacteriochlorophylls, vol. 18, pp. 257–284, Elsevier, London, ISBN 978-0-12-521518-9, https://doi.org/10.1016/s0580-9517(08)70478-1, 1985.

Orosa, M., Torres, E., Fidalgo, P., and Abalde, J.: Production and analysis of secondary carotenoids in green algae, Journal of Applied Phycology, 12, 553–556, https://doi.org/10.1023/a:1008173807143, 2000.

O'Connell, D. W., Mark Jensen, M., Jakobsen, R., Thamdrup, B., Joest Andersen, T., Kovacs, A., and Bruun Hansen, H. C.: Vivianite formation and its role in phosphorus retention in Lake Ørn, Denmark, Chemical Geology, 409, 42–53, https://doi.org/10.1016/j.chemgeo.2015.05.002, 2015.

Pennington, F., Haxo, F., Borch, G., and Liaaen-Jensen, S.: Carotenoids of cryptophyceae, Biochemical Systematics and Ecology, 13, 215–219, https://doi.org/10.1016/0305-1978(85)90029-8, 1985.

https://doi.org/10.5194/egusphere-2026-1390
Preprint. Discussion started: 20 March 2026

Pestryakova, L. A., Herzschuh, U., Gorodnichev, R., and Wetterich, S.: The sensitivity of diatom taxa from Yakutian lakes (north-eastern Siberia) to electrical conductivity and other environmental variables, Polar Research, 37, 1485 625, https://doi.org/10.1080/17518369.2018.1485625, 2018.

Pniewski, F.: HPLC separation of cyanobacterial and algal photosynthetic pigments, Biologia, 75, 223–233, https://doi.org/10.2478/s11756-019-00407-8, 2020.

Puddick, J., Naeher, S., Pearman, J. K., Page, C. D., Romanazzi, D., Schallenberg, L. A., Howarth, J. D., Vandergoes, M. J., and Wood, S. A.: Characterizing carotenoids in cyanobacterial cultures – Opportunities and implications for paleolimnological studies, Harmful Algae, 127, 102 481, https://doi.org/10.1016/j.hal.2023.102481, 2023.

Rein, B. and Sirocko, F.: In-situ reflectance spectroscopy - analysing techniques for high-resolution pigment logging in sediment cores, International Journal of Earth Sciences, 91, 950–954, https://doi.org/10.1007/s00531-002-0264-0, 2002.

Reinig, F., Wacker, L., Jöris, O., Oppenheimer, C., Guidobaldi, G., Nievergelt, D., Adolphi, F., Cherubini, P., Engels, S., Esper, J., Land, A., Lane, C., Pfanz, H., Remmele, S., Sigl, M., Sookdeo, A., and Büntgen, U.: Precise date for the Laacher See eruption synchronizes the Younger Dryas, Nature, 595, 66–69, https://doi.org/10.1038/s41586-021-03608-x, 2021.

Rothe, M., Kleeberg, A., and Hupfer, M.: The occurrence, identification and environmental relevance of vivianite in waterlogged soils and aquatic sediments, Earth-Science Reviews, 158, 51–64, https://doi.org/10.1016/j.earscirev.2016.04.008, 2016.

Roy, S., Llewellyn, C. A., Egeland, E. S., and Johnsen, G., eds.: Phytoplankton Pigments: Characterization, Chemotaxonomy and Applications in Oceanography, Cambridge Environmental Chemistry Series, Cambridge University Press, Cambridge, ISBN 978-1-107-00066-7, https://doi.org/10.1017/cbo9780511732263, 2011.

Ruth, U., Wagenbach, D., Steffensen, J. P., and Bigler, M.: Continuous record of microparticle concentration and size distribution in the central Greenland NGRIP ice core during the last glacial period, Journal of Geophysical Research: Atmospheres, 108, https://doi.org/10.1029/2002JD002376, 2003.

Schmidt, R., Psenner, R., Müller, J., Indinger, P., and Kamenik, C.: Impact of late glacial climate variations on stratification and trophic state of the meromictic lake Längsee (Austria): validation of a conceptual model by multi proxy studies, Journal of Limnology, 61, 49, https://doi.org/10.4081/jlimnol.2002.49, 2002.

Schmincke, H.-U.: Vulkane der Eifel: Aufbau, Entstehung und heutige Bedeutung, Spektrum Akademischer Verlag, Heidelberg, ISBN 978-3827423665, 2007.

Schmitt, L., Kirnbauer, T., Angerer, T., Volkmann, R., Roddatis, V., Wirth, R., and Klein, S.: Genesis of Devonian volcanic-associated Lahn-Dill-type iron ores — part I: iron mobilisation and mineralisation style, Mineralium Deposita, 59, 1777–1801, https://doi.org/10.1007/s00126-023-01218-3, 2023.

Schneider, T., Rimer, D., Butz, C., and Grosjean, M.: A high-resolution pigment and productivity record from the varved Ponte Tresa basin (Lake Lugano, Switzerland) since 1919: insight from an approach that combines hyperspectral imaging and high-performance liquid chromatography, Journal of Paleolimnology, 60, 381–398, https://doi.org/10.1007/s10933-018-0028-x, 2018.

Scholtysik, G., Goldhammer, T., Arz, H. W., Moros, M., Littke, R., and Hupfer, M.: Geochemical focusing and burial of sedimentary iron, manganese, and phosphorus during lake eutrophication, Limnology and Oceanography, 67, 768–783, https://doi.org/10.1002/lno.12019, 2022.

Schouten, S. J., Schmidhauser, N. R. M. M., Grosjean, M., Lami, A., Boltshauser-Kaltenrieder, P., van Leeuwen, J. F. N., Vogel, H., and Zahajská, P.: Lake anoxia, primary production, and algal community shifts in response to rapid climate changes during the Late Glacial, Biogeosciences, 22, 3821–3842, https://doi.org/10.5194/bg-22-3821-2025, 2025.

https://doi.org/10.5194/egusphere-2026-1390
Preprint. Discussion started: 20 March 2026

Schouten, S. J., Grosjean, M., Zander, P. D., Schmidhauser, N. R., Tu, L., Lami, A., Vogel, H., van Leeuwen, J., and Zahajská, P.: Climate-eutrophication-anoxia interactions in Late Glacial Soppensee, Switzerland: Forcings, non-linear responses and recovery, Quaternary Science Reviews, 375, 109 804, https://doi.org/10.1016/j.quascirev.2026.109804, 2026.

Schwefel, R., Gaudard, A., Wüest, A., and Bouffard, D.: Effects of climate change on deepwater oxygen and winter mixing in a deep lake (Lake Geneva): Comparing observational findings and modeling, Water Resources Research, 52, 8811–8826, https://doi.org/10.1002/2016wr019194, 2016.

Senger, H., Wagner, C., Hermsmeier, D., Hohl, N., Urbig, T., and Bishop, N. I.: The influence of light intensity and wavelength on the contents of α- and β-carotene and their xanthophylls in green algae, Journal of Photochemistry and Photobiology B: Biology, 18, 273–279, https://doi.org/10.1016/1011-1344(93)80075-k, 1993.

Simpson, D. J. and Smith, K. M.: Structures and transformations of the bacteriochlorophylls e and their bacteriopheophorbides, Journal of the American Chemical Society, 110, 1753–1758, https://doi.org/10.1021/ja00214a016, 1988.

Slomp, C. P., Epping, E. H. G., Helder, W., and Raaphorst, W. V.: A key role for iron-bound phosphorus in authigenic apatite formation in North Atlantic continental platform sediments, Journal of Marine Research, 54, 1179–1205, https://doi.org/10.1357/0022240963213745, 1996.

Smith, D., Scott, J., Steele, A., Cody, G., Ohara, S., and Fogel, M.: Effects of Metabolism and Physiology on the Production of Okenone and Bacteriochlorophyllain Purple Sulfur Bacteria, Geomicrobiology Journal, 31, 128–137, https://doi.org/10.1080/01490451.2013.815293, 2013.

Sobek, S., Tranvik, L. J., Prairie, Y. T., Kortelainen, P., and Cole, J. J.: Patterns and regulation of dissolved organic carbon: An analysis of 7,500 widely distributed lakes, Limnology and Oceanography, 52, 1208–1219, https://doi.org/10.4319/lo.2007.52.3.1208, 2007.

Spanbauer, T. L., Allen, C. R., Angeler, D. G., Eason, T., Fritz, S. C., Garmestani, A. S., Nash, K. L., and Stone, J. R.: Prolonged instability prior to a regime shift in a shallow lake, PLoS ONE, 9, e108 936, https://doi.org/10.1371/journal.pone.0108936, 2014.

Strickland, J. and Parsons, T.: A Practical Handbook of Seawater Analysis, 2nd edition., https://doi.org/10.25607/OBP-1791, 1972.

Sugita, S., Gaillard, M.-J., and Broström, A.: Landscape openness and pollen records: a simulation approach, The Holocene, 9, 409–421, https://doi.org/10.1191/095968399666429937, 1999.

Søndergaard, M., Jensen, J. P., and Jeppesen, E.: Role of sediment and internal loading of phosphorus in shallow lakes, Hydrobiologia, 506–509, 135–145, https://doi.org/10.1023/b:hydr.0000008611.12704.dd, 2003.

Takaichi, S. and Mochimaru, M.: Carotenoids and carotenogenesis in cyanobacteria: unique ketocarotenoids and carotenoid glycosides, Cellular and Molecular Life Sciences, 64, 2607–2619, https://doi.org/10.1007/s00018-007-7190-z, 2007.

Tonolla, M., Peduzzi, R., and Hahn, D.: Long-Term Population Dynamics of Phototrophic Sulfur Bacteria in the Chemocline of Lake Cadagno, Switzerland, Applied and Environmental Microbiology, 71, 3544–3550, https://doi.org/10.1128/aem.71.7.3544-3550.2005, 2005.

Tu, L., Zander, P., Szidat, S., Lloren, R., and Grosjean, M.: The influences of historic lake trophy and mixing regime changes on long-term phosphorus fraction retention in sediments of deep eutrophic lakes: a case study from Lake Burgäschi, Switzerland, Biogeosciences, 17, 2715–2729, https://doi.org/10.5194/bg-17-2715-2020, 2020.

Tu, L., Gilli, A., Lotter, A. F., Vogel, H., Moyle, M., Boyle, J. F., and Grosjean, M.: The nexus among long-term changes in lake primary productivity, deep-water anoxia, and internal phosphorus loading, explored through analysis of a 15,000-year varved sediment record, Global and Planetary Change, 207, 103 643, https://doi.org/10.1016/j.gloplacha.2021.103643, 2021.

https://doi.org/10.5194/egusphere-2026-1390
Preprint. Discussion started: 20 March 2026

Vila, X., Abella, C., Figueras, J., and Hurley, J.: Vertical models of phototrophic bacterial distribution in the metalimnetic microbial communities of several freshwater North-American kettle lakes, FEMS Microbiology Ecology, 25, 287–299, https://doi.org/10.1111/j.1574-6941.1998.tb00481.x, 1998.

Vossel, H., Reed, J. M., Houk, V., Cvetkoska, A., and Van de Vijver, B.: Cyclotella paleo-ocellata, a new centric diatom (Bacillariophyta) from Lake Kinneret (Israel), Fottea, 15, 63–75, https://doi.org/10.5507/FOT.2015.006, 2015.

Weltje, G. J. and Tjallingii, R.: Calibration of XRF core scanners for quantitative geochemical logging of sediment cores: Theory and application, Earth and Planetary Science Letters, 274, 423–438, https://doi.org/10.1016/j.epsl.2008.07.054, 2008.

Wienhues, G., Zahajská, P., Fischer, D., Schneider, T., and Grosjean, M.: Direct detection of phycocyanin in sediments by hyperspectral imaging, Journal of Paleolimnology, 73, 73–87, https://doi.org/10.1007/s10933-024-00350-y, 2025.

Wienhues, G., Vogel, H., Tylmann, W., and Grosjean, M.: Late Holocene deforestation and reforestation controls lake mixing regimes and aquatic ecology: Lessons from anthropogenic disturbances in NE Poland, Anthropocene, 53, 100 517, https://doi.org/10.1016/j.ancene.2025.100517, 2026.

Witz, G. and michaelh00: guiwitz/napari-sediment: v0.4.0, https://doi.org/10.5281/zenodo.14932597, 2025.

Woolway, R. I. and Merchant, C. J.: Worldwide alteration of lake mixing regimes in response to climate change, Nature Geoscience, 12, 271–276, https://doi.org/10.1038/s41561-019-0322-x, 2019.

Zahajská, P.: Holzmaar sediment data cleaning, processing and visualisation, GitHub, Zenodo, https://renkulab.io/p/snsf-anoxia-project/holzmaar, 2026.

Zander, P. D., Żarczyński, M., Tylmann, W., Rainford, S.-k., and Grosjean, M.: Seasonal climate signals preserved in biochemical varves: insights from novel high-resolution sediment scanning techniques, Climate of the Past, 17, 2055–2071, https://doi.org/10.5194/cp-17-2055-2021, 2021a.

Zander, P. D., Żarczyński, M., Vogel, H., Tylmann, W., Wacnik, A., Sanchini, A., and Grosjean, M.: A high-resolution record of Holocene primary productivity and water-column mixing from the varved sediments of Lake Żabińskie, Poland, Science of The Total Environment, 755, 143 713, https://doi.org/10.1016/j.scitotenv.2020.143713, 2021b.

Zander, P. D., Wienhues, G., and Grosjean, M.: Scanning hyperspectral imaging for in situ biogeochemical analysis of lake sediment cores: Review of recent developments, Journal of imaging, 8, 58, https://doi.org/10.3390/jimaging8030058, publisher: MDPI, 2022.

Zander, P. D., Wirth, S. B., Gilli, A., Peduzzi, S., and Grosjean, M.: Hyperspectral imaging sediment core scanning tracks high-resolution Holocene variations in (an) oxygenic phototrophic communities at Lake Cadagno, Swiss Alps, Biogeosciences, 20, 2221–2235, https://doi.org/10.5194/bg-20-2221-2023, 2023.

Zander, P. D., Böhl, D., Sirocko, F., Auderset, A., Haug, G. H., and Martínez-García, A.: Reconstruction of warm-season temperatures in central Europe during the past 60 000 years from lacustrine branched glycerol dialkyl glycerol tetraethers (brGDGTs), Climate of the Past, 20, 841–864, https://doi.org/10.5194/cp-20-841-2024, 2024.

Zolitschka, B.: A 14,000 year sediment yield record from western Germany based on annually laminated lake sediments, Geomorphology, 22, 1–17, https://doi.org/10.1016/S0169-555X(97)00051-2, 1998.

Zolitschka, B., Brauer, A., Negendank, J. F., Stockhausen, H., and Lang, A.: Annually dated late Weichselian continental paleoclimate record from the Eifel, Germany, Geology, 28, 783–786, https://doi.org/10.1130/0091-7613(2000)028<0783:adlwcp>2.3.co;2, 2000.

Züllig, H.: Carotenoids from plankton and photosynthetic bacteria in sediments as indicators of trophic changes in Lake Lobsigen during the last 14000 years, Hydrobiologia, 143, 315–319, https://doi.org/10.1007/bf00026676, 1986.

https://doi.org/10.5194/egusphere-2026-1390
Preprint. Discussion started: 20 March 2026

Züllig, H.: Role of carotenoids in lake sediments for reconstructing trophic history during the late Quaternary, vol. 2, pp. 191–208, Springer Netherlands, ISBN 9789400926554, https://doi.org/10.1007/978-94-009-2655-4_12, 1989.

Żarczyński, M., Wacnik, A., and Tylmann, W.: Tracing lake mixing and oxygenation regime using the Fe/Mn ratio in varved sediments: 2000year-long record of human-induced changes from Lake Żabińskie (NE Poland), Science of The Total Environment, 657, 585–596, https://doi.org/10.1016/j.scitotenv.2018.12.078, 2019.

Appendix A: The napari-sediment workflow

napari-sediment workflow consists of three main components which follow the original workflow by Butz et al. (2015):

(1) Image Loading and Preprocessing: Raw hyperspectral data stored in ENVI HDR format were imported and normalized using white and dark reference images. An interactive masking tool allowed manual annotation of corrupted regions (e.g., core breaks, edge effects, or moisture artifacts) that were excluded from subsequent analysis. Region-of-interest (ROI) selection tools enabled focusing analysis on specific core sections or depths.

(2) Dimensionality Reduction: To reduce data volume and computational complexity while retaining diagnostic spectral features, two complementary dimensionality reduction approaches were applied. *Spectral dimensionality reduction* was performed using Minimum Noise Fraction (MNF) transformation, which maximizes the signal-to-noise ratio by separating signal from noise through two successive principal component analyses. The first transformation decorrelates and rescales the noise in the data, and the second decorrelates the noise-whitened data. MNF components are ordered by decreasing signal-to-noise ratio, with the first components containing coherent spectral information and later components dominated by noise. *Spatial dimensionality reduction* employed pixel purity index (PPI) algorithms to identify spectrally pure pixels representing distinct sediment facies. These pure pixels were subsequently clustered to identify representative spectral endmembers.

(3) Spectral Index Calculation and Mapping: After endmember identification, spectral indices (RABD, RABA) were calculated based on characteristic absorption features. The software enabled interactive selection of wavelength ranges for baseline definition and absorption minimum identification. Index maps were generated showing the spatial distribution of each index across the core, and 1D projection profiles were extracted by averaging index values across user-defined ROI widths. These profiles were optionally smoothed using Savitzky-Golay filtering with adjustable window sizes. All processed data, including index maps, projection profiles, and endmember spectra, were exported for statistical analysis and calibration.

The interactive nature of napari-sediment provided several advantages: (i) real-time visualization of preprocessing effects enabled quality control at each processing step, (ii) manual masking allowed expert knowledge to guide data cleaning, (iii) interactive ROI selection facilitated targeted analysis of specific sedimentary features, and (iv) the ability to iteratively adjust spectral index parameters optimized signal detection for specific pigments. The software architecture, built on the napari viewer framework, enabled GPU-accelerated rendering of large hyperspectral datasets and seamless integration with Python scientific libraries (NumPy, SciPy, scikit-learn) for advanced data analysis.

https://doi.org/10.5194/egusphere-2026-1390
Preprint. Discussion started: 20 March 2026

Appendix B: Construction of the Holzmaar Late Glacial stacked pollen record

To provide a continuous palynological context for the 2019 Holzmaar (HZM) sediment sequence, we integrated pollen datasets from Litt and Stebich (1999) and Litt et al. (2009). These records were derived from cores collected in 1992 (Litt, 2025) and 1996 (Litt, 2010), respectively. The integration into the 2019 master chronology followed a two-step alignment process:

1. Section-to-Core Correlation (1992 Core to 2019 Master)

The pollen data from the 1992 campaign Litt and Stebich (1999) were originally available only on a depth scale within individual core sections (specifically sections **HZM92 1a–6u, 2b–5o, and 2b–5u**). To be able to use these data, we needed to first transfer these data on our 2019 individual cores, and then we could assign our age-depth model (VT22, Birlo et al. (2023)) to these data. As expected, the 1992 and 2019 coring locations differed, localized stratigraphic stretching and compression were observed.

- **Correlation method:** We performed a visual lithostratigraphic correlation using high-resolution core photographs. Distinctive marker layers and varve patterns served as tie-points to align these individual 1992 sections with the 2019 individual cores, and fuhrer to the HMZ19 composite depth.
- **Transformation:** This alignment allowed us to transfer the 2019 age-depth model to the 1992 sampling depths, synchronizing the pollen counts with our new high-resolution geochemical and pigment datasets as well as with the complementary, but lower resolution pollen data from Litt et al. (2009).

2. Multi-core stacking (1996 core)

The pollen data from the 1996 core (Litt et al., 2009) were available only on a calibrated age scale.

- **Integration:** Once the 1992 data were successfully migrated to the 2019 age scale (VT22), we stacked the two datasets (cores from 1992 and 1996) based on their age scale.
- **Result:** This produced a comprehensive stacked pollen record for Holzmaar, anchored to the 2019 chronology and depth scale. This approach minimizes stratigraphic gaps and provides a framework for interpreting vegetation-driven changes in lake stratification.

https://doi.org/10.5194/egusphere-2026-1390
Preprint. Discussion started: 20 March 2026

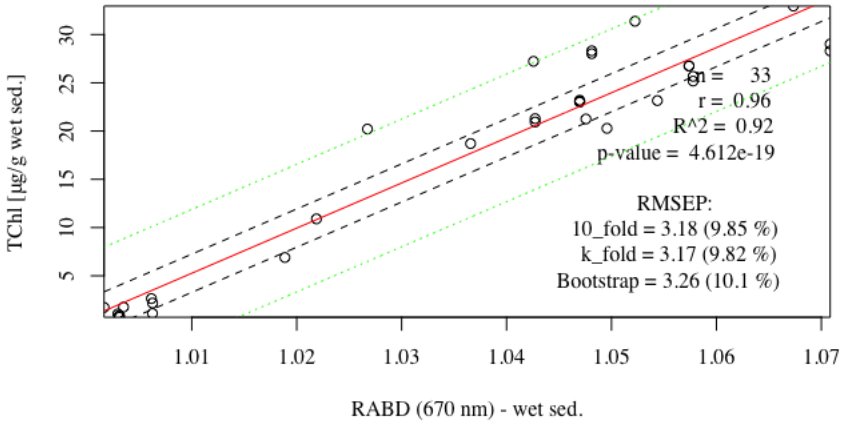

Figure A1. Calibration and validation of the hyperspectral chlorophyll proxy. Linear regression model establishing the quantitative relationship between the spectral index (RABD_{671}; Relative Absorption Band Depth at 671 nm measured on wet sediment) and spectrophotometrically determined Total Chlorophyll concentrations ($\mu g \cdot g^{-1}_{\mathrm{wetsed.}}$). The model demonstrates a strong linear correlation ($R^2 = 0.92$, $p < 0.001$, $n = 33$), validating RABD_{671} as a robust high-resolution proxy for primary production. The red line represents the linear fit, while the black dashed and green dotted lines indicate the 95% confidence and prediction intervals, respectively. Cross-validation (RMSEP) indicates a prediction error of approximately 3.2 $\mu g \cdot g^{-1}$ ($\sim 10\%$).

https://doi.org/10.5194/egusphere-2026-1390
Preprint. Discussion started: 20 March 2026

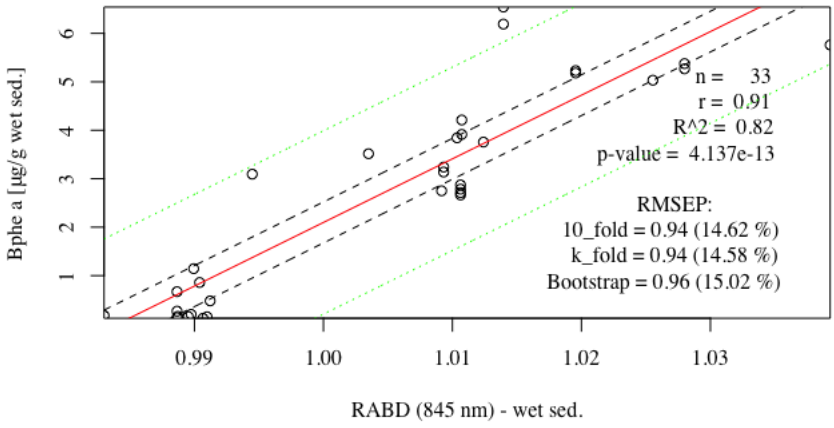

Figure A2. Calibration and validation of the hyperspectral bacteriopheophytin *a* proxy. Linear regression model establishing the quantitative relationship between the spectral index (RABD_{845}; Relative Absorption Band Depth at 845 nm measured on wet sediment) and spectrophotometrically determined bacteriopheophytin *a* concentrations ($\mu g \cdot g^{-1}_{\mathrm{wetsed.}}$). The model demonstrates a strong linear correlation ($R^2 = 0.82$, $p < 0.001$, $n = 33$), validating RABD_{845} as a robust high-resolution proxy for purple sulphur bacteria (PSB) abundance. The red line represents the linear fit, while the black dashed and green dotted lines indicate t he 95% confidence and prediction intervals, respectively. Cross-validation (RMSEP) indicates a prediction error of approximately $0.94\ \mu g \cdot g^{-1}$ ($\sim 14.6\%$), confirming the proxy's sensitivity for detecting anoxia-driven pigment layers.

https://doi.org/10.5194/egusphere-2026-1390
Preprint. Discussion started: 20 March 2026

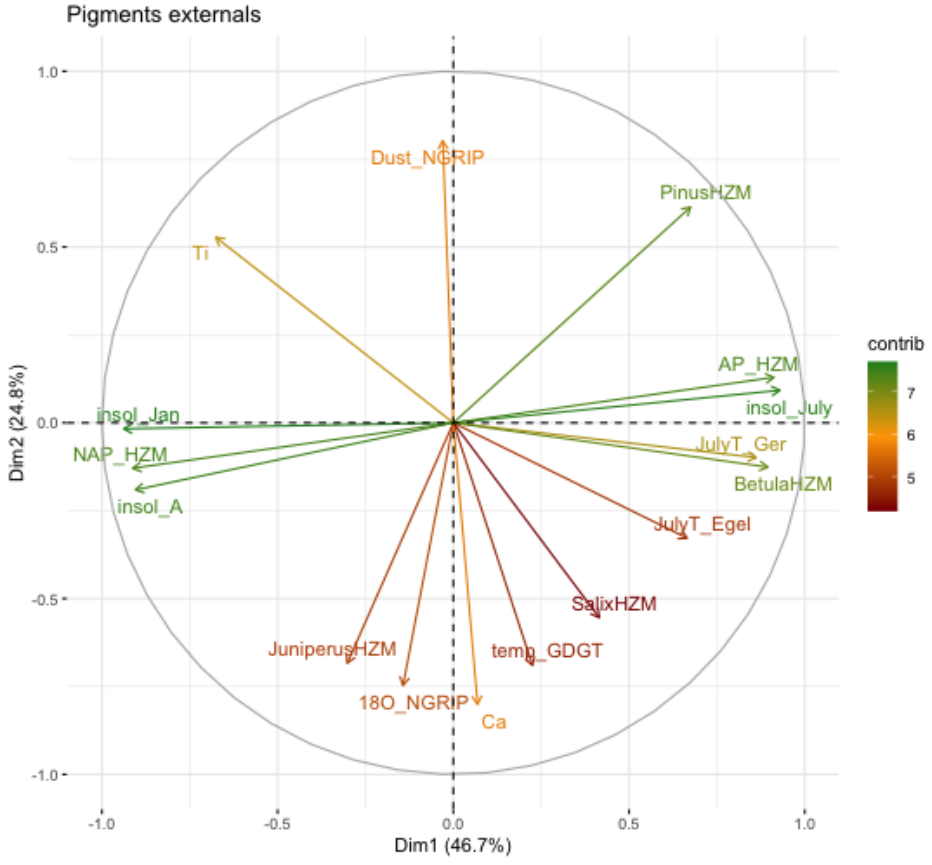

Figure A3. The biplot displays the correlation structure among the independent proxies considered for the Redundancy Analysis (RDA), revealing the primary environmental gradients driving the system. The first axis (Dim1, 46.7%) represents the dominant climatic and vegetational gradient. It strongly opposes indicators of warmth and forest development (positive loadings: *Betula*, *Pinus*, Summer Insolation, Regional Temperatures) against markers of cold, open steppe environments (negative loadings: Non-Arboreal Pollen (NAP), *Juniperus*, Winter Insolation). The second axis (Dim2, 24.8%) captures the sedimentological signal, distinguishing allochtonous detrital inputs (positive loadings: Ti, NGRIP Dust) from autochthonous carbonate precipitation (negative loading: Ca) and regional temperature signals ($\delta^{18}O_{NGRIP}$). This analysis demonstrates the high collinearity between local vegetation and regional temperature records, justifying the selection of a reduced subset of non-redundant variables for the final RDA model.

https://doi.org/10.5194/egusphere-2026-1390
Preprint. Discussion started: 20 March 2026

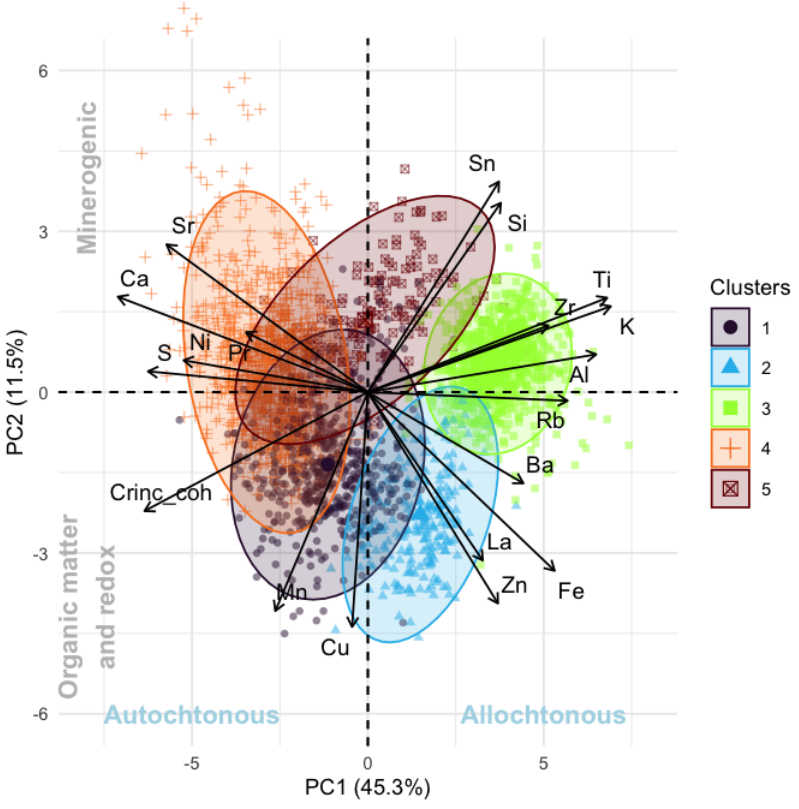

Figure A4. Principal Component Analysis (PCA) variable correlation plot of high-resolution XRF geochemical data. The biplot displays the loading vectors of elemental proxies to the first two principal components. The first principal component (PC1) explains 45.3% of the total variance and represents the gradient between allochtonous catchment inputs and autochthonous lake production. It separates detrital/siliciclastic elements (strong positive loadings: Ti, K, Zr, Al, Si, Rb) from elements associated with endogenic carbonate precipitation (strong negative loadings: Ca, Sr). The second principal component (PC2) explains 11.5% of the variance, primarily distinguishing detrital minerals from elements associated with organic matter binding and redox cycling (positive loadings: Mn, S, Cu, Zn, and coherent scattering $Cr_{inc/coh}$). This analysis validates the use of Ti as a robust proxy for detrital/minerogenic material supply and Ca and Mn as indicators of in-lake geochemical processes. The ellipses and their colours correspond to the unconstrained cluster displayed in Figure 1.

https://doi.org/10.5194/egusphere-2026-1390
Preprint. Discussion started: 20 March 2026

Figure A5. Stratigraphic trajectory of sedimentary pigment assemblages in PCA space (PC1 vs. PC3). The scatterplot displays the temporal evolution of the phototrophic community, with sample scores connected in chronological order. Points are coloured by stratigraphic zone: Pleniglacial (green circle), Bølling (orange triangle), Allerød (purple square), and Younger Dryas (pink cross). The large red and green dots mark specific time markers (ages in cal yr BP) to indicate the direction of change. The trajectory reveals the reversibility of the primary producer community. The transition from the Bølling to the Allerød involves a shift toward negative PC1 and negative PC3 values, a region defined by the dominance of okenone (purple sulphur bacteria; see Figure 2). The subsequent transition to the Younger Dryas marks a return toward the positive PC1 space and positive PC3 (generalist/pioneer pigments), indicating the breakdown of stable euxinia and the recovery of the oxic/mixed community structure.

https://doi.org/10.5194/egusphere-2026-1390
Preprint. Discussion started: 20 March 2026

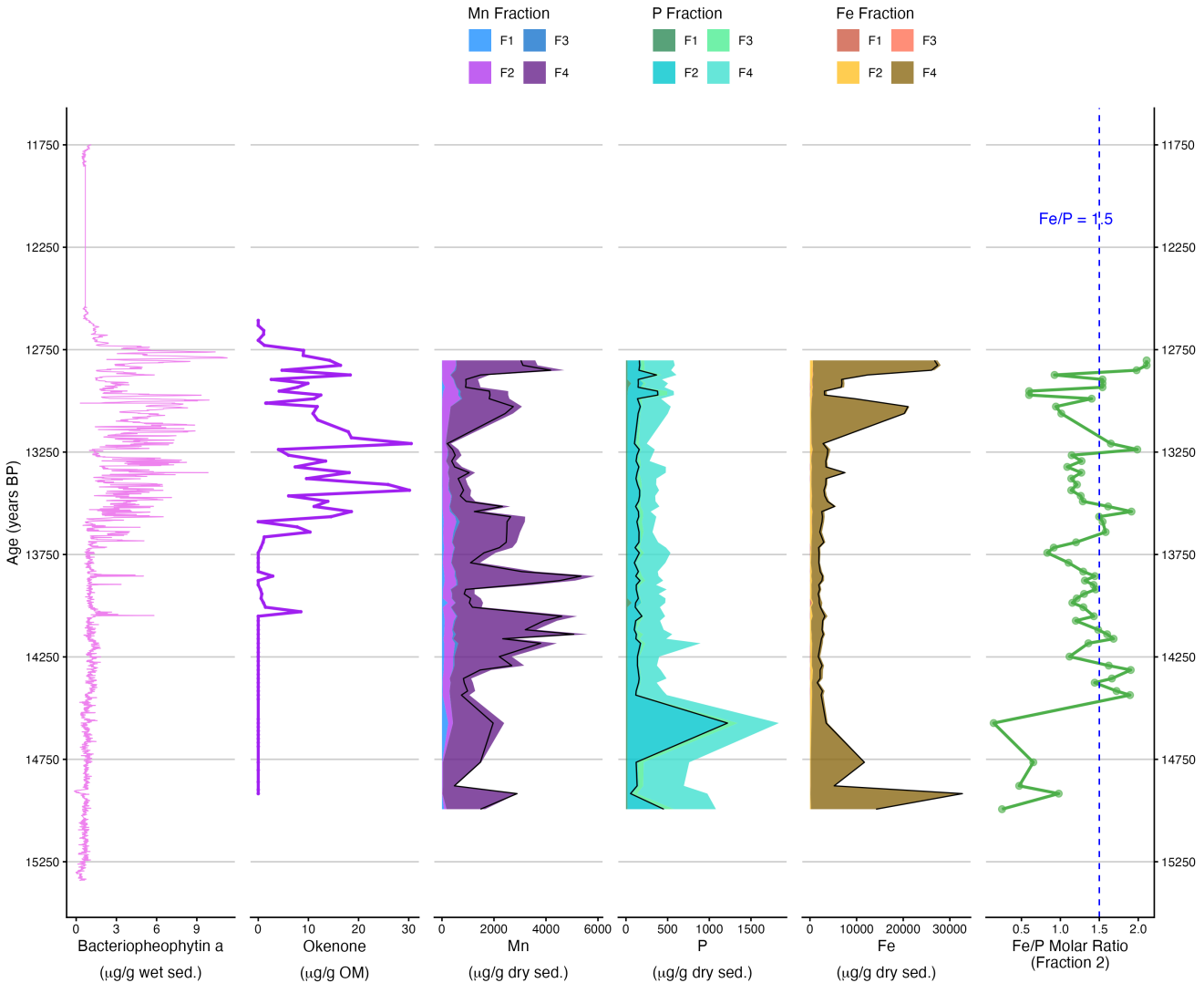

Figure A6. Fe, Mn and P fractions with the anoxic indicators: okenone and calibrated RABD845. Fe:P ratio of the fractions 2 are used to interpret what form of Fe and P we have present. Fe:P < 1, iron limitation, P in F2 can be present as organic bound P; if S present (okenone), Fe is bound as pyrite (FeS_2) and not available to bound with P. Fe:P between 1.5-2.5 is vivianite, Fe:P > 2.5, iron excess, likely to be bound as siderite or iron oxides.

https://doi.org/10.5194/egusphere-2026-1390
Preprint. Discussion started: 20 March 2026

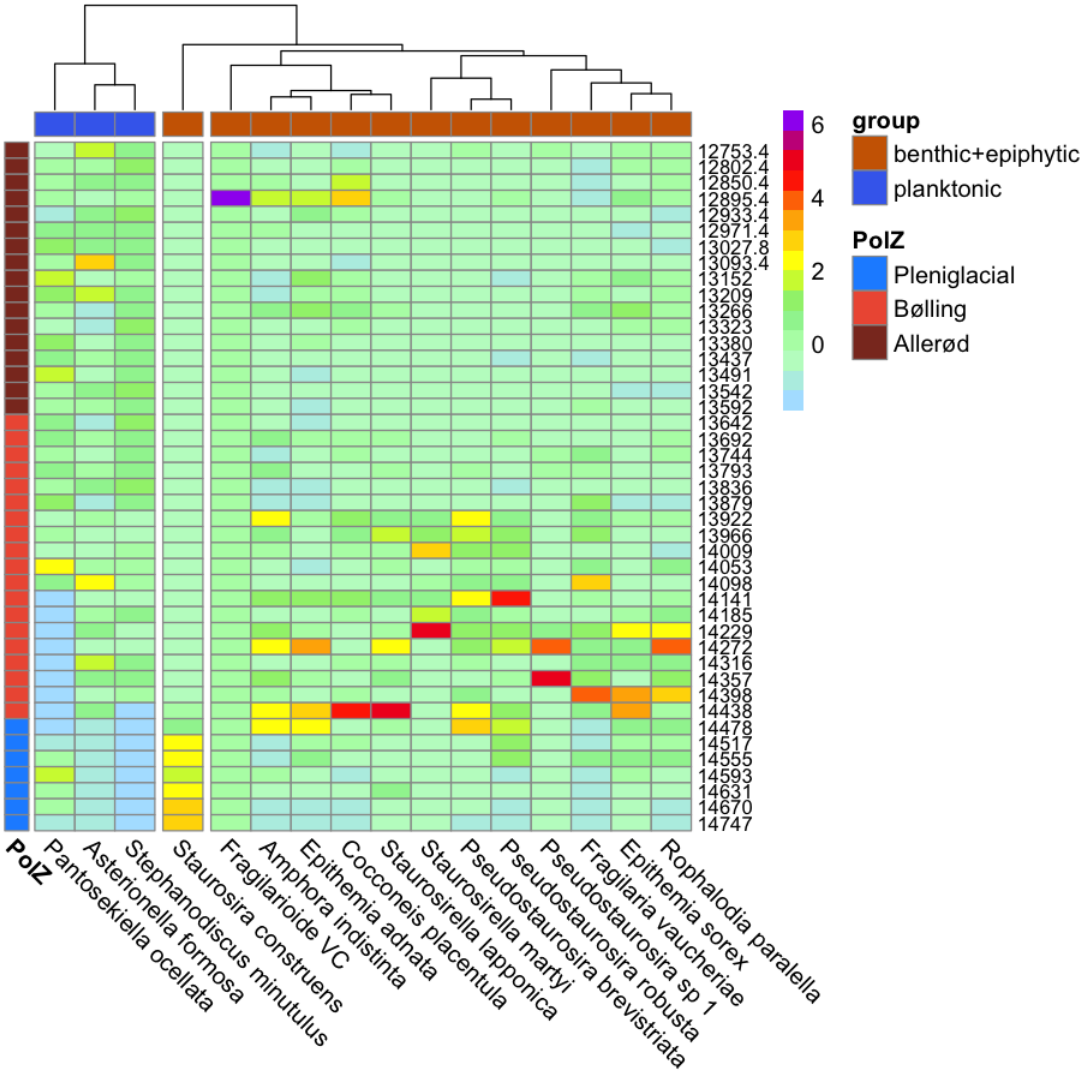

Figure A7. Clustered heatmap of diatom taxa abundance across Late Glacial. Rows represent individual samples with their age (cal yr BP, right side), and columns represent individual diatom species. Taxa are categorized by ecological niche (planktonic vs. benthic+epiphytic) and clustered by similarity in occurrence patterns (correlation/euclidean distance). Left-side annotation (PolZ) indicates the pollen zones: Pleniglacial, Bølling, and Allerød. Colour intensity represents relative abundance (scaled).

https://doi.org/10.5194/egusphere-2026-1390
Preprint. Discussion started: 20 March 2026

Table A1. Sedimentary pigments identified in Holzmaar, their taxonomic affinities, and key references.

Pigment	Biological interpretation (Producer group)	References
Oxygenic Phototrophs (General & Algal)		
Chlorophyll-*a*	Total oxygenic biomass (all algae and cyanobacteria)	Roy et al. (2011); Deshpande et al. (2014); Leavitt and Hodgson (2002)
Phaeophytin-*a*	Degradation product of Chl-*a* (anoxic preservation)	Leavitt and Hodgson (2002); Guilizzoni and Lami (2003)
Phaeophorbide-*a*	Degradation product of Chl-*a* (grazing indicator)	Lami et al. (1994); Bianchi and Canuel (2011)
Cyanobacteria		
Echinenone	General cyanobacteria (specific marker)	Roy et al. (2011); Puddick et al. (2023)
Canthaxanthin	Filamentous/Colonial cyanobacteria (N-fixing)	Senger et al. (1993); Orosa et al. (2000); Takaichi and Mochimaru (2007); Deshpande et al. (2014); Roy et al. (2011); Puddick et al. (2023)
Zeaxanthin	Cyanobacteria and some Green algae	Senger et al. (1993); Roy et al. (2011); Deshpande et al. (2014); Puddick et al. (2023)
Diatoms & Chrysophytes (Silicifiers)		
Fucoxanthin	Diatoms, Chrysophytes, Dinoflagellates	Roy et al. (2011); Bertrand (2010)
Diatoxanthin	Diatoms (light stress indicator)	Roy et al. (2011); Bertrand (2010)
Diadinoxanthin	Dinoflagellates, Diatoms, Green algae	Roy et al. (2011); Lami et al. (2000)
Green algae & Cryptophytes		
Lutein	Green algae (Chlorophytes), euglinids	Senger et al. (1993); Orosa et al. (2000); Roy et al. (2011)
Alloxanthin	Cryptophytes (often associated with Silicifiers)	Pennington et al. (1985); Lotter (2001)
α-Carotene	Green algae	Roy et al. (2011); Senger et al. (1993); Orosa et al. (2000)
β-Carotene	General phototrophs (algal production)	Roy et al. (2011); Makri et al. (2018)
Anoxygenic phototrophs (bacterial)		
Bacteriochlorophyll *a*	Total anoxygenic Phototrophs (PSB, PNSB, GSB)	Oelze (1985)
Bacteriopheophytin *a*	Purple sulphur bacteria (*Chromatiaceae*)	Smith et al. (2013); Coolen and Overmann (1998)
Okenone *a*	Purple sulphur bacteria (*Chromatiaceae*)	Züllig (1986); Coolen and Overmann (1998)
Isorenieratene	Green sulphur bacteria (*Chlorobiaceae*)	Züllig (1989); Vila et al. (1998)
Bacteriopheophytin *e*	Green sulphur bacteria (*Chlorobiaceae*)	Biebl and Pfennig (1978); Simpson and Smith (1988); Chen et al. (2001); Glaeser et al. (2002)
OH-Spheroidene	Purple non-sulphur bacteria (*Rhodospirillaceae*)	Zander et al. (2023); Albrecht et al. (1997); Davies et al. (1969)